

1 Scaling regimes and linear / nonlinear responses of last 2 millennium climate to volcanic and solar forcings

3 S. Lovejoy¹, and C. Varotsos²

4 ¹Physics, McGill University, 3600 University St., Montreal, Que., Canada

5 ²Climate Research Group, Division of Environmental Physics and Meteorology, Faculty of Physics, University of Athens,
6 University Campus Bldg. Phys. V, Athens 15784, Greece

7 Correspondence to: S. Lovejoy (lovejoy@physics.mcgill.ca) and C. Varotsos (covar@phys.uoa.gr)

8

9 **Abstract.** At scales much longer than the deterministic predictability limits (about 10 days), the statistics of the atmosphere
10 undergoes a drastic transition, the high frequency weather acts as a random forcing on the lower frequency macroweather. In
11 addition, up to decadal and centennial scales the equivalent radiative forcings of solar, volcanic and anthropogenic perturbations
12 are small compared to the mean incoming solar flux. This justifies the common practice of reducing forcings to radiative
13 equivalents (which are assumed to combine linearly), as well as the development of linear stochastic models, including for
14 forecasting at monthly to decadal scales.

15 In order to clarify the validity of the linearity assumption and determine its scale range, we use last Millennium simulations, both
16 with the simplified Zebiac- Cane (ZC) model and the NASA GISS E2-R fully coupled GCM. We systematically compare the
17 statistical properties of solar only, volcanic only and combined solar and volcanic forcings over the range of time scales from one
18 to 1000 years. We also compare the statistics to multiproxy temperature reconstructions. The main findings are: a) that the
19 variability of the ZC and GCM models are too weak at centennial and longer scales, b) for longer than ≈ 50 years, the solar and
20 volcanic forcings combine subadditively (nonlinearly) compounding the weakness of the response, c) the models display another
21 nonlinear effect at shorter time scales: their sensitivities are much higher for weak forcing than for strong forcing (their
22 intermittencies are different) and we quantify this with statistical scaling exponents.

23 1. Introduction

24 1.1 Linearity versus nonlinearity

25 The GCM approach to climate modeling is based on the idea that whereas weather is an initial value problem, the climate is a
26 boundary value problem (Bryson, 1997; Pielke, 1998). This means that although the weather's sensitive dependence on initial
27 conditions (chaos, the "butterfly effect") leads to a loss of predictability at time scales of about 10 days, nevertheless averaging
28 over enough "weather" leads to a convergence to the model's "climate". This climate is thus the state to which averages of model
29 outputs converge for fixed atmospheric compositions and boundary conditions (i.e. control runs).

30 The question then arises as to the response of the system to small changes in the boundary conditions: for example
31 anthropogenic forcings are less than 2 W/m^2 , and at least over scales of several years, solar and volcanic forcings are of similar
32 magnitude or smaller (see e.g. Fig. 1a and the quantification in Fig. 2). These numbers are of the order of 1% of the mean solar
33 radiative flux so that we may anticipate that the atmosphere responds fairly linearly. This is indeed that usual assumption and it

34 justifies the reduction of potentially complex forcings to overall radiative forcings (see Meehl et al., 2004 for GCM
 35 investigations at annual scales and Hansen et al., 2005 for greenhouse gases). However, at long enough scales, linearity clearly
 36 breaks down, indeed starting with the celebrated “Daisy world” model (Watson and Lovelock, 1983), there is a whole literature
 37 that uses energy balance models to study the strongly nonlinear interactions/feedbacks between global temperatures and albedoes.
 38 There is no debate that temperature-albedo feedbacks are important at the multimillennial scales of the glacial- interglacial
 39 transitions. While some authors (e.g. Roques et al., 2014) use time scales as short as 200 years for the critical ice-albedo
 40 feedbacks, others have assumed that the temperature response to solar and volcanic forcings over the last millennium are
 41 reasonably linear (e.g. Østvand et al., 2014; Rypdal and Rypdal, 2014), while Pelletier (1998) and Fraedrich et al., (2009) assume
 42 linearity to even longer scales.

43 It is therefore important to establish the times scales over which linear responses are a reasonable assumption. However,
 44 clearly even over scales where typical responses to small forcings are relatively linear, the response may be nonlinear if the
 45 forcing is – volcanic or volcanic- like, i.e. if it is sufficiently “spikey” or intermittent.

46 **1.2 Atmospheric variability: scaling regimes**

47 Before turning our attention to models, what can we learn empirically? Certainly, at high enough frequencies (the weather
 48 regime), the atmosphere is highly nonlinear. However, at about ten days, the atmosphere undergoes a drastic transition to a lower
 49 frequency regime, and this “macroweather” regime is potentially quasi- linear in its responses. Indeed, the basic atmospheric
 50 scaling regimes were identified some time ago - primarily using spectral analysis (Lovejoy and Schertzer, 1986; Pelletier, 1998;
 51 Shackleton and Imbrie, 1990; Huybers and Curry, 2006). However, the use of real space fluctuations provided a clearer picture
 52 and a simpler interpretation. It also showed that the usual view of atmospheric variability, as a sequence of narrow scale range
 53 processes (e.g. nonlinear oscillators), has seriously neglected the main source of variability, namely the scaling “background
 54 spectrum” (Lovejoy, 2014). What was found is that for virtually all atmospheric fields, there was a transition from the behavior
 55 of the mean temperature fluctuations scaling $\langle \Delta T(\Delta t) \rangle \approx \Delta t^H$ with $H > 0$ to a lower frequency scaling regime with $H < 0$ at scales
 56 $\Delta t \approx 10$ days; the macroweather regime. The transition scale of around 10 days, can be theoretically predicted on the basis of
 57 the scaling of the turbulent wind due to solar forcing (via the imposed energy rate density; see (Lovejoy and Schertzer, 2010;
 58 Lovejoy and Schertzer, 2013; Lovejoy et al., 2014). Whereas the weather is naturally identified with the high frequency $H > 0$
 59 regime and with temperature values “wandering” up and down like a drunkard’s walk, the lower frequency $H < 0$ regime is
 60 characterized by fluctuations tending to cancel out – effectively starting to converge. This converging regime is a low frequency
 61 type of weather, described as “macroweather” (Lovejoy, 2013; Lovejoy et al., 2014). For the GCM control runs, macroweather
 62 effectively continues to asymptotically long times; in the real world, it continues to time scales of 10-30 years (industrial) and
 63 50-100 years (pre-industrial) after which a new $H > 0$ regime is observed; it is natural to associate this new regime with the
 64 climate (see Fig. 5 of Lovejoy et al., 2013; see also Franzke et al., 2013). Other papers analyzing macroweather scaling include
 65 Koscielny-Bunde et al., (1998); Eichner et al., (2003); Kantelhardt et al., (2006); Rybski et al., (2006); Bunde et al., (2005);
 66 Østvand et al., (2014); Rypdal and Rypdal, (2014); Fredriksen and Rypdal, (2015).

67 The explanation for the “macroweather” to climate transition (at scale τ_c) appears to be that over the “macroweather” time
 68 scales - where the fluctuations are “cancelling” - other, slow processes which presumably include both external climate forcings
 69 and other slow (internal) land-ice or biogeochemical processes – become stronger and stronger. At some point (τ_c) their

70 variability dominates. A significant point where opinions diverge is the value of the global transition scale τ_c during the
 71 preindustrial Holocene; and the possibility that there are large regional variations in τ_c during the Holocene so that Greenland
 72 ice core data may not be globally representative, see Lovejoy (2015a) for a discussion.

73 **1.3 Scaling in the numerical models**

74 There have been several studies of the low frequency control run responses of GCMs (Vyushin et al., 2004; Zhu et al., 2006;
 75 Fraedrich et al., 2009; Lovejoy et al., 2013; Fredriksen and Rypdal, 2015) finding that they are scaling down to their lowest
 76 frequencies. This scaling is a consequence of the absence of a characteristic time scale for the long-time model convergence; it
 77 turns out that the relevant scaling exponents are very small: empirically the GCM convergence is “ultra slow” (Lovejoy et al.,
 78 2013) (section 3.4). Most earlier studies focused on the implications of the long – range statistical dependencies implicit in the
 79 scaling statistics. Unfortunately, due to this rather technical focus, the broader implications of the scaling have not been widely
 80 appreciated.

81 More recently, using scaling fluctuation analysis, behavior has been put into the general theoretical framework of GCM
 82 climate modeling (Lovejoy et al., 2013). From the scaling point of view, it appears that the climate arises as a consequence of
 83 slow internal climate processes combined with external forcings (especially volcanic and solar - and in the recent period -
 84 anthropogenic forcings). From the point of view of the GCMs, the low frequency (multicentennial) variability arises exclusively
 85 as a response to external forcings, although potentially - with the addition of (known or currently unknown) slow processes such
 86 as land-ice or biogeochemical processes - new internal sources of low frequency variability could be included. Ignoring the
 87 recent (industrial) period, and confining ourselves to the last millennium, the key question for GCM models is whether or not
 88 they can reproduce the climate regime where the decline of the “macroweather” fluctuations ($H < 0$) is arrested and the increasing
 89 $H > 0$ climate regime fluctuations begin. In a recent publication (Lovejoy et al., 2013), four GCMs simulating the last millennium
 90 were statistically analyzed and it was found that their low frequency variability (especially below $(100 \text{ yrs})^{-1}$) was somewhat
 91 weak, and this was linked to both the weakness of the solar forcings (when using sunspot-based solar reconstructions with $H > 0$),
 92 and – for strong volcanic forcings - with the statistical type of the forcing ($H < 0$, Lovejoy and Schertzer, 2012a; Bothe et al.,
 93 2013a,b; Zanchettin et al., 2013; see also Zanchettin et al., 2010 for the dynamics on centennial time scales).

94 **1.4 This paper**

95 The weakness of the responses to solar and volcanic forcings at multicentennial scales raises question a linearity question: is the
 96 response of the combined (solar plus volcanic) forcing roughly the sum of the individual responses? Additivity is often implicitly
 97 assumed when climate forcings are reduced to their equivalent radiative forcings and Mann et al., (2005) already pointed out that
 98 – at least - in the Zebiac-Cane (ZC) model discussed below that they are not additive. Here we more precisely analyze this
 99 question and quantify the degree of sub-additivity as a function of temporal scale (section 3.4). A related linear/nonlinear issue
 100 pointed out by Clement et al., (1996), is that due to the nonlinear model response, there is a high sensitivity to a small forcing
 101 and a low sensitivity to a large forcing. Systems in which strong and weak events have different statistical behaviors display
 102 stronger or weaker “clustering” and are often termed “intermittent” (from turbulence). When they are also scaling, the weak and
 103 strong events are characterized by different scaling exponents that quantify how the respective clustering changes with scale. In
 104 section 4, we investigate this quantitatively and confirm that it is particularly strong for volcanic forcing, and that for the ZC

105 model the response (including that of a GCM), is much less intermittent, implying that the model strongly (and
 106 nonlinearly) smooths the forcing.

107 In this paper, we establish analysis methodologies that can address these issues and apply them to model outputs that
 108 cover the the required range of time scales: Last Millenium model outputs. Unfortunately - although we consider the NASA
 109 GISS E2-R Last Millenium simulations, there seem to be no full Last Millenium GCM simulations that have the entire suite of
 110 volcanic only, solar only and solar plus volcanic forcings and responses, therefore we have use the simplified Zebiak-Cane
 111 model outputs published by Mann et al., (2005) (and even this lacked control runs to directly quantify the internal variability).

112 Although the Zebiak –Cane model lacks several important mechanisms- notably for our purposes deep ocean dynamics -
 113 there are clearly sources of low frequency variability present in the model. For example, Goswami and Shukla, (1991) using 360
 114 year control runs found multidecadal and multicentennial nonlinear variability due to the feedbacks between SST anomalies, low
 115 level convergence and atmospheric heating. In addition, in justifying his Millenium ZC simulations, (Mann et al., 2005)
 116 specifically cited model centennial scale variability as a factor motivating their study.

117 **2. Data and analysis**

118 **2.1 Discussion**

119 During the pre-industrial part of the last millennium, the atmospheric composition was roughly constant, and the earth's orbital
 120 parameters varied by only a small amount. The main forcings used in GCM climate models over this period are thus solar and
 121 volcanic (in the GISS-E2-R simulations discussed below, reconstructed land use changes are also simulated but the
 122 corresponding forcings are comparatively weak and will not be discussed further). In particular, the importance of volcanic
 123 forcings was demonstrated by Minnis et al., (1993) who investigated the volcanic radiative forcing caused by the 1991 eruption
 124 of Mount Pinatubo, and found that volcanic aerosols produced a strong cooling effect. Later, Shindell et al., (2003) used a
 125 stratosphere-resolving general circulation model to examine the effect of the volcanic aerosols and solar irradiance variability on
 126 pre-industrial climate change. They found that the best agreement with historical and proxy data was obtained using both
 127 forcings. However, solar and volcanic forcings induce different responses because the stratospheric and surface influences in the
 128 solar case reinforce one another but in the volcanic case they are opposed. In addition, there are important differences in solar
 129 and volcanic temporal variabilities (including seasonality) that statistically link volcanic eruptions with the onset of ENSO events
 130 (Mann et al., 2005). Decreased solar irradiance cools the surface and stratosphere (Cracknell and Varotsos 2007, 2011;
 131 Kondratyev and Varotsos, 1995a,b). In contrast, volcanic eruptions cool the surface, but aerosol heating warms the sunlit lower
 132 stratosphere (Shindell et al., 2003; Miller et al., 2012). This leads to an increased meridional gradient in the lower stratosphere,
 133 but a reduced gradient in the tropopause region (Chandra et al., 1996; Varotsos et al., 1994, 2009).

134 Vyushin et al., (2004) suggested that volcanic forcings improve the low frequency variability scaling performance of
 135 atmosphere-ocean models compared to all other forcings (see however the comment by Blender and Fraedrich, (2004), which
 136 also discusses earlier papers on the field e.g. Fraedrich and Blender, (2003); Blender and Fraedrich, (2004). Weber, (2005) used
 137 a set of simulations with a climate model, driven by reconstructed forcings in order to study the Northern Hemisphere
 138 temperature response to volcanic and solar forcing, during 1000-1850. It was concluded that the response to solar forcing
 139 equilibrates at interdecadal timescales, while the response to volcanic forcing never equilibrates due to the fact that the time

140 interval between volcanic eruptions is typically shorter than the dissipation time scale of the climate system (in fact they
 141 are scaling so that eruptions occur over all observed time scales, see below).

142 At the same time, Mann et al. (2005) investigated the response of El Niño to natural radiative forcing changes during
 143 1000-1999, by employing the Zebiak–Cane model for the coupled ocean–atmosphere system in the tropical Pacific. They found
 144 that the composite feedback of the volcanic and solar radiative forcing to past changes, reproduces the fluctuations in the
 145 variability of the historic El Niño records (e.g., Efstathiou et al., 2011; Varotsos 2013).

146 Finally, as discussed below Lovejoy and Schertzer, (2012a) analysed the time scale dependence of several solar
 147 reconstructions Lean, (2000); Wang et al., (2005); Krivova et al., (2007); Steinhilber et al., (2009); Shapiro et al., (2011) and the
 148 two main volcanic reconstructions Crowley, (2000) and Gao et al., (2008), (referred to as “Crowley” and “Gao” in the following).
 149 The solar forcings were found to be qualitatively quite different depending on whether the reconstructions were based on
 150 sunspots or ^{10}Be isotopes from ice cores with the former increasing with time scale and the latter decreasing with time scale. This
 151 quantitative and qualitative difference brings into question the reliability of the solar reconstructions. By comparison, the two
 152 volcanic reconstructions were both statistically similar in type; they were very strong at annual and sometimes multiannual scales
 153 but they quickly decrease with time scale ($H < 0$) explaining why they are weak at centennial and millennial scales. We re-
 154 examine these findings below.

155 2.2 The climate simulation of Mann et al. (2005) using the Zebiak–Cane model

156 Mann et al., (2005) used the Zebiak–Cane model of the tropical Pacific coupled ocean – atmosphere system (Zebiak and Cane,
 157 1987) to produce a 100-realization ensemble for solar forcing only, volcanic forcing only and combined forcings over the last
 158 millennium. Figure 1a shows the forcings and mean responses of the model which were obtained from:
 159 ftp://ftp.ncdc.noaa.gov/pub/data/paleo/climate_forcing/mann2005/mann2005.txt. No anthropogenic effects were included. Mann
 160 et al., (2005) modeled the region between $\pm 30^\circ$ of latitude - by scaling the Crowley volcanic forcing reconstruction with a
 161 geometric factor 1.57 to take the limited range of latitudes into account. Figure 1b shows the corresponding GISS-E2-R
 162 simulation responses for three different forcings as discussed in Schmidt et al., (2013) and Lovejoy et al., (2013). Although these
 163 were averaged over the northern hemisphere land only (a somewhat different geography than the ZC simulations), one can see
 164 that the low frequencies seem similar even if the high frequencies are somewhat different. We quantify this below.

165 3. Methods

166 3.1 Comparing simulations with observations as functions of scale

167 The ultimate goal of weather and climate modelling (including forecasting) is to make simulations $T_{sim}(t)$ as close as possible
 168 to observations $T_{obs}(t)$. Ignoring measurement errors and simplifying the discussion by only considering a single spatial
 169 location (i.e. a single time series), the goal is to achieve simulations with $T_{sim}(t) = T_{obs}(t)$. However, this is not only very ambitious
 170 for the simulations, even when considering the observations, $T_{obs}(t)$ is often difficult to evaluate if only because data are often
 171 sparse or inadequate in various ways. However, a necessary condition for $T_{sim}(t) = T_{obs}(t)$ is the weaker statistical equality:

172 $T_{sim}(t) \stackrel{d}{=} T_{obs}(t)$ where “ $\stackrel{d}{=}$ ” means equal in probability distributions (we can say that $a = b$ if $\text{Pr}(a > s) = \text{Pr}(b > s)$ where “ Pr ”

173 indicates “probability”). Although $T_{sim}(t) = T_{obs}(t)$ is only a necessary (but not sufficient) condition for
 174 $T_{sim}(t) \stackrel{d}{=} T_{obs}(t)$, it is much easier to empirically verify.

175 Starting in the 1990s, with the advent of ensemble forecasting systems, the Rank Histogram (RH) method was proposed
 176 (Anderson, 1996) as a simple nonparametric test of $T_{sim}(t) \stackrel{d}{=} T_{obs}(t)$, and this has led to a large literature, including recently
 177 Bothe et al., (2013a, b). From our perspective there are two limitations of the RH method. First, it is non-parametric so that its
 178 statistical power is low. More importantly, it essentially tests the equation $T_{sim}(t) \stackrel{d}{=} T_{obs}(t)$ at a single unique time scale/resolution.
 179 This is troublesome since the statistics of both $T_{sim}(t)$ and $T_{obs}(t)$ series will depend on their space-time resolutions; recall
 180 that averaging in space alters the temporal statistics, e.g. $5^\circ \times 5^\circ$ data are not only spatially, but also are effectively temporally
 181 smoothed with respect to $1^\circ \times 1^\circ$ data. This means that even if $T_{sim}(t)$ and $T_{obs}(t)$ have nominally the same temporal resolutions
 182 they may easily have different high frequency variability. Possibly more importantly - as claimed in Lovejoy et al., (2013) and
 183 below - the main difference between $T_{sim}(t)$ and $T_{obs}(t)$ may be that the latter has more low frequency variability than the
 184 former, and this will not be captured by the RH technique which operates only at the highest frequency available. This problem
 185 is indirectly acknowledged, see for example the discussion of correlations in Marzban et al., (2011). The potential significance of
 186 the low frequencies becomes obvious when $H > 0$ for the low frequency range. In this case – since the series tends to “wander”,
 187 small differences in the low frequencies may translate into very large differences in RH, and this even if the high frequencies are
 188 relatively accurate.

189 A straightforward solution is to use the same basic idea – i.e. to change the sense of equality from deterministic to
 190 probabilistic (“=” to “ $\stackrel{d}{=}$ ”) – but to compare the statistics systematically over a range of time scales. The simplest way is to
 191 check the equality $\Delta T_{sim}(\Delta t) \stackrel{d}{=} \Delta T_{obs}(\Delta t)$ where ΔT is the fluctuation of the temperature over a time period Δt (see the discussion
 192 in Lovejoy and Schertzer, (2013) box 11.1). In general, knowledge of the probabilities is equivalent to knowledge of (all) the
 193 statistical moments (including the non-integer ones), and for technical reasons it turns out to be easier to check
 194 $\Delta T_{sim}(\Delta t) \stackrel{d}{=} \Delta T_{obs}(\Delta t)$ by considering the statistical moments.

195 3.2 Scaling Fluctuation Analysis

196 In order to isolate the variability as a function of time scale Δt , we estimated the fluctuations $\Delta F(\Delta t)$ (forcings, W/m^2),
 197 $\Delta T(\Delta t)$ (responses, K). Although it is traditional (and often adequate) to define fluctuations by absolute differences
 198 $\Delta T(\Delta t) = |T(t + \Delta t) - T(t)|$, for our purposes this is not sufficient. Instead we should use the absolute difference of the means from
 199 t to $t + \Delta t/2$ and from $t + \Delta t/2$ to $t + \Delta t$. Technically, the latter corresponds to defining fluctuations using Haar wavelets rather
 200 than “poor man’s” wavelets (differences). In a scaling regime, the fluctuations vary with the time lag in a power law manner:

$$201 \Delta T = \varphi \Delta t^H \quad (1)$$

202 where ϕ is a controlling dynamical variable (e.g. a dynamical flux) whose mean $\langle \phi \rangle$ is independent of the lag Δt (i.e.
 203 independent of the time scale). This means that the behaviour of the mean fluctuation is $\langle \Delta T \rangle \approx \Delta t^H$ so that when $H > 0$, on
 204 average fluctuations tend to grow with scale whereas when $H < 0$, they tend to decrease. Note that the symbol “ H ” is in honour of
 205 Harold Edwin Hurst (Hurst, 1951). Although in the case of quasi-Gaussian statistics, it is equal to his eponymous exponent, the
 206 H used here is valid in the more general multifractal case and is generally different.

207 Fluctuations defined as differences are adequate for fluctuations increasing with scale ($H > 0$). When $H > 0$, the rate at
 208 which average differences increase with time lag Δt directly reflects the increasing importance of low frequencies with respect
 209 to high frequencies. However, in physical systems the differences tend to increase even when $H < 0$. This is because correlations
 210 $\langle T(t+\Delta t)T(t) \rangle$ tend to decrease with the time lag Δt and this directly implies that the mean square differences $\langle \Delta T(\Delta t)^2 \rangle$
 211 increase (mathematically, for a stationary process: $\langle \Delta T(\Delta t)^2 \rangle = \langle (T(t+\Delta t) - T(t))^2 \rangle = 2(\langle T^2 \rangle - \langle T(t+\Delta t)T(t) \rangle)$). This means that when
 212 $H < 0$, differences cannot correctly characterize the fluctuations. For $H < 0$ the high-frequency details dominate the differences
 213 and prevent these differences to decrease with increasing scale Δt .

214 The Haar fluctuation which is useful for $-1 < H < 1$ is particularly easy to understand since with proper “calibration” in
 215 regions where $H > 0$, its value can be made to be very close to the difference fluctuation, while in regions where $H < 0$, it can be
 216 made close to another simple to interpret “anomaly fluctuation”. The latter is simply the temporal average of the series over a
 217 duration Δt of the series with its overall mean removed (in Lovejoy and Schertzer, 2012b this was termed a “tendency”
 218 fluctuation which is a less intuitive term). In this case, the decrease of the Haar fluctuations for increasing lag Δt characterizes
 219 how effectively averaging a (mean zero) process (the anomaly) over longer time scales reduces its variability. Here, the
 220 calibration is affected by multiplying the raw Haar fluctuation by a factor of 2 which brings the values of the Haar fluctuations
 221 very close to both the corresponding difference and anomaly fluctuations (over time scales with $H > 0$, $H < 0$ respectively). This
 222 means that in regions where $H > 0$, to good accuracy, the Haar fluctuations can be treated as differences whereas in regions where
 223 $H < 0$ they can be treated as anomalies. While other techniques such as Detrended Fluctuation Analysis (Peng et al., 1994)
 224 perform just as well for determining exponents, they have the disadvantage that their fluctuations are not at all easy to interpret
 225 (they are the standard deviations of the residues of polynomial regressions on the running sum of the original series). Indeed, the
 226 DFA fluctuation function is typically presented without any units.

227 Once estimated, the variation of the fluctuations with time scale can be quantified by using their statistics; the q^{th} order
 228 structure function $S_q(\Delta t)$ is particularly convenient:

$$229 \quad S_q(\Delta t) = \langle \Delta T(\Delta t)^q \rangle \quad (2)$$

230 where “ $\langle \rangle$ ” indicates ensemble averaging (here, we average over all disjoint intervals of length Δt). Note that although q can
 231 in principle be any value, here we restrict to $q > 0$ since divergences may occur – indeed for multifractals, are expected - for $q < 0$).
 232 In a scaling regime, $S_q(\Delta t)$ is a power law:

$$233 \quad S_q(\Delta t) = \langle \Delta T(\Delta t)^q \rangle \propto \Delta t^{\xi(q)}, \quad \xi(q) = qH - K(q) \quad (3)$$

234 where the exponent $\xi(q)$ has a linear part qH and a generally nonlinear and convex part $K(q)$ with $K(1)=0$. $K(q)$
 235 characterizes the strong non Gaussian, multifractal variability; the “intermittency”. Gaussian processes have $K(q)=0$. The root-
 236 mean-square (RMS) variation $S_2(\Delta t)^{1/2}$ (denoted simply $S(\Delta t)$ below) has the exponent $\xi(2)/2=H-K(2)/2$. It is only when
 237 the intermittency is small ($K(q) \approx 0$) that we have $\xi(2)/2 \approx H = \xi(1)$. Note that since the spectrum is a second order statistic, we
 238 have the useful relationship for the exponent β of the power law spectra: $\beta=1+\xi(2)=1+2H-K(2)$ (this is a corollary of the Wiener-
 239 Khintchin theorem). Again, only when $K(2)$ is small do we have the commonly used relation $\beta \approx 1+2H$; in this case, $H > 0$, $H < 0$
 240 corresponds to $\beta > 1$, $\beta < 1$, respectively. To get an idea of the implications of the nonlinear $K(q)$, note that a high q value
 241 characterizes the scaling of the strong events whereas a low q characterizes the scaling of the weak events (q is not restricted to
 242 integer). The scalings are different whenever the strong and weak events cluster to different degrees, the clustering in turn is
 243 precisely determined by another exponent - the codimension - which is itself is uniquely determined by $K(q)$. We return to the
 244 phenomenon of “intermittency”, in section 4, it is particularly pronounced in the case of volcanic forcings.

245 Figure 2a shows the result of estimating the Haar fluctuations for the solar and volcanic forcings. The solar reconstruction
 246 that was used is a hybrid obtained by “splicing” the annual resolution sunspot based reconstruction (Fig. 2b, top; back to 1610,
 247 although only the more recent part was used by Mann et al. (2005) with a ^{10}Be based reconstruction (Fig. 2b, bottom) at much
 248 lower resolution ($\approx 40\text{-}50$ yrs). In Fig. 2a, the two rightmost curves are for two different ^{10}Be reconstructions; at any given time
 249 scale, their amplitudes differ by nearly a factor of 10 yet they both have Haar fluctuations that diminish with scale ($H \approx -0.3$).
 250 Figure 2b (top) clearly shows the qualitative difference with “wandering” ($H > 0$, sunspot based) and Fig. 2b (bottom), the
 251 cancelling ($H < 0$, ^{10}Be based) solar reconstructions (Lovejoy and Schertzer, 2012a). In the “spliced” reconstruction used here,
 252 the early ^{10}Be part (1000-1610) at low resolution was interpolated to annual resolution; the interpolation was close to linear so
 253 that we find $H \approx 1$ over the scale range 1-50 yrs, with the $H < 0$ part barely visible over the range 100-600 years (roughly the
 254 length of the ^{10}Be part of the reconstruction).

255 The reference lines in Fig. 2a have slopes -0.4, -0.3, 0.4 showing that both solar and volcanic forcings are fairly accurately
 256 scaling (although because of the “splicing” for the solar, only up until $\approx 200\text{-}300$ yrs) but with exactly opposite behaviours:
 257 whereas the solar fluctuations increase with time scale, the volcanic fluctuations decrease with scale. For time scales beyond
 258 200-300 yrs, the solar forcing is stronger than the volcanic forcing (they “cross” at roughly 0.3 W/m^2).

259 3.3 Linearity and nonlinearity

260 There is no question that - at least in the usual deterministic sense - the atmosphere is turbulent and nonlinear. Indeed, the ratio of
 261 the nonlinear to the linear terms in the dynamical equations – the Reynolds number - is typically about 10^{12} . Due to the smaller
 262 range of scales, in the numerical models it is much lower, but it is still $\approx 10^3$ to 10^4 . Indeed it turns out that the variability builds
 263 up scale by scale from large to small scales so that - since the dissipation scale is about 10^{-3} m - the resulting (millimetre scale)
 264 variability can be enormous; the statistics of this buildup are quite accurately modelled by multifractal cascades (see the review
 265 Lovejoy and Schertzer, 2013, especially ch. 4 for cascade analyses of data and model outputs). The cascade based Fractionally
 266 Integrated Flux model (FIF, Schertzer and Lovejoy, 1987) is a nonlinear stochastic model of the weather scale dynamics, and can

267 be extended to provide nonlinear stochastic models of the macroweather and climate regimes (Lovejoy and Schertzer,
 268 2013, ch. 10).

269 However, ever since Hasselmann, (1976), it has been proposed that sufficiently space-time averaged variables may
 270 respond linearly to sufficiently space-time averaged forcings. In the resulting (low frequency) phenomenological models, the
 271 nonlinear deterministic (high frequency) dynamics act as a source of random perturbations; the resulting stochastic model is
 272 usually taken as being linear. Such models are only justified if there is a physical scale separation between the high frequency
 273 and low frequency processes. The existence of a relevant break (at 2- 10 day scales) has been known since Panofsky and Van der
 274 Hoven, (1955) and was variously theorized as the “scale of migratory pressure systems of synoptic weather map scale” (Van der
 275 Hoven, 1957) and later as the “synoptic maximum” (Kolesnikov and Monin, 1965). From the point of view of Hasselman-type
 276 linear stochastic modelling (now often referred to as “Linear Inverse Modelling (LIM)”, e.g., Penland and Sardeshmukh, (1995);
 277 Newman et al., (2003); Sardeshmukh and Sura, (2009)), the system is regarded as a multivariate Ornstein-Uhlenbeck (OU)
 278 process. At high frequencies, an OU process is essentially the integral of a white noise (with spectrum $\omega^{-\beta_h}$ with $\beta_h = 2$),
 279 whereas at low frequencies it is a white noise, (i.e. $\omega^{-\beta_l}$ with $\beta_l = 0$). In the LIM models, these regimes correspond to the
 280 weather and macroweather, respectively. Recently Newman, (2013) has shown predictive skill for global temperature hindcasts
 281 is somewhat superior to GCM’s for 1-2 year horizons.

282 In the more general scaling picture going back to Lovejoy and Schertzer, (1986), the transition corresponds to the lifetime
 283 of planetary structures. This interpretation was quantitatively justified in (Lovejoy and Schertzer, 2010) by using the turbulent
 284 energy rate density. The low and high frequency regimes were scaling and had spectra significantly different than those of OU
 285 processes (notably with $0.2 < \beta_l < 0.8$) with the two regimes now being referred to as “weather” and “macroweather” (Lovejoy and
 286 Schertzer, 2013). Indeed, the main difference with respect to the classical LIM is at low frequencies. Although the difference in
 287 β_l may not seem so important, the LIM value $\beta_l = 0$, (white noise) has no low frequency predictability whereas the actual values
 288 $0.2 < \beta_l < 0.8$ (depending mostly on the land or ocean location) corresponds to potentially huge predictability (the latter can
 289 diverge as β_l approaches 1). A new “ScalIng Macroweather Model” (SLIMM) has been proposed as a set of fractional order (but
 290 still linear) stochastic differential equations with predictive skill for global mean temperatures out to at least 10 years (Lovejoy et
 291 al., 2015; Lovejoy, 2015b). However, irrespective of the exact statistical nature of the weather and macroweather regimes, a
 292 linear stochastic model may still be a valid approximation over significant ranges.

293 These linear stochastic models (whether LIM or SLIMM) explicitly exploit the weather/macroweather transition and may have
 294 some skill up to macroweather scales perhaps as large as decades. However, at long enough time scales, another class of
 295 phenomenological model is often used, wherein the dynamics are determined by radiative energy balances. Energy balance
 296 models focus on slower (true) climate scale processes such as sea ice – albedo feedbacks and are generally quite nonlinear, being
 297 associated with nonlinear features such as tipping points and bifurcations (Budyko, 1969). These models are typically zero or one
 298 dimensional in space (i.e. they are averaged over the whole earth or over latitude bands) and may be deterministic or stochastic
 299 (see Nicolis, 1988 for an early comparison of the two approaches). See Dijkstra, (2013) for a survey of the classical deterministic
 300 dynamical systems approach as well as the more recent stochastic “random dynamical systems” approach, (see also Ragone, et
 301 al., 2014). Although energy balance models are almost always nonlinear, there have been several suggestions that linear energy
 302 balance models are in fact valid up to millennial and even multimillennial scales.

303 Finally, we could mention the existence of empirical evidence of stochastic linearity between forcings and
 304 responses in the macroweather regime. Such evidence comes for example, from the apparent ability of linear regressions to
 305 “remove” the effects of volcanic, solar and anthropogenic forcings (Lean and Rind, 2008). This has perhaps been quantitatively
 306 demonstrated in the case of anthropogenic forcing where use is made of the globally, annually averaged CO₂ radiative forcings
 307 (as a linear surrogate for all anthropogenic forcings). When this radiative forcing was regressed against similarly averaged
 308 temperatures, it gave residues with amplitudes $\pm 0.109\text{K}$ (Lovejoy, 2014a) which is almost exactly the same as GCM estimates of
 309 the natural variability (e.g., Laepple et al., (2008)). Notice that in this case the identification of the global temperature T_{globe} as
 310 the sum of a regression determined anthropogenic component (T_{anth}) with residues as natural variability (T_{nat}) is in fact only
 311 a confirmation of *stochastic* linearity (i.e. $T_{globe}^d = T_{anth} + T_{nat}$). Since presumably the actual residues would have been different
 312 if there had been no anthropogenic forcing. Indeed, when the residues were analysed using fluctuation analysis, it was only their
 313 statistics that were close to the pre-industrial multiproxy statistics.

314 3.4 Testing linearity: the additivity of the responses

315 We can now test the linearity of the model responses to solar and volcanic forcings. First consider the model responses (Fig. 3a).
 316 Compare the response to the volcanic only forcing (green) curve; with the response from the solar only forcing (black). As
 317 expected from Fig. 2a, the former is stronger than the latter up (until centennial scales) reflecting the stronger volcanic forcing.
 318 At scales $\Delta t \approx 100$ yrs however, we see that the solar only has a stronger response, also as expected from Fig. 2a. Now
 319 consider the response to the combined volcanic and solar forcing (brown). Unsurprisingly, it is very close to the volcanic only
 320 until $\Delta t \approx 100$ yrs; however at longer time scales, the combined response seems to decrease following the volcanic forcing
 321 curve; it seems that at these longer time scales the volcanic and solar forcings have negative feedbacks so that the combined
 322 response to solar plus volcanic forcing is actually less than for pure solar forcing, they are “subadditive”.

323 In order to quantify this we can easily determine the expected solar and volcanic response if the two were combined
 324 additively (linearly). In the latter case, the solar and volcanic fluctuations would not interfere with each other, and since these
 325 forcings are statistically independent, the responses would also be statistically independent, the response variances would add.

326 A linear response means that temperature fluctuations due to only solar forcing ($\Delta T_s(\Delta t)$) and only volcanic forcing
 327 ($\Delta T_v(\Delta t)$) would be related to the temperature fluctuations of the response to the combined solar plus volcanic forcings
 328 ($\Delta T_{s,v}(\Delta t)$) as:

$$329 \Delta T_{s,v}(\Delta t) = \Delta T_s(\Delta t) + \Delta T_v(\Delta t) \quad (4)$$

330 This is true regardless of the exact definition of the fluctuation: as long as the fluctuation is defined by a linear operation on the
 331 temperature series any wavelet will do. Therefore, squaring both sides and averaging (“ $\langle \rangle$ ”) and assuming that the fluctuations
 332 in the solar and volcanic forcings are statistically independent of each other (i.e., $\langle \Delta T_s(\Delta t) \Delta T_v(\Delta t) \rangle = 0$), we obtain:

$$333 \langle \Delta T_{s,v}(\Delta t)^2 \rangle = \langle \Delta T_s(\Delta t)^2 \rangle + \langle \Delta T_v(\Delta t)^2 \rangle \quad (5)$$

334 The implied additive response structure function $S(\Delta t) = \left(\langle \Delta T_s(\Delta t)^2 \rangle + \langle \Delta T_v(\Delta t)^2 \rangle \right)^{1/2}$ is shown in Fig. 3b along with
 335 the ratio of the latter to the actual (nonlinear) solar plus volcanic response (top: $\left(\langle \Delta T_s(\Delta t)^2 \rangle + \langle \Delta T_v(\Delta t)^2 \rangle \right)^{1/2} / \left(\langle \Delta T_{s,v}(\Delta t)^2 \rangle^{1/2} \right)$). It can be
 336 seen that the ratio is fairly close to unity for time scales below about 50 yrs. However beyond 50 yrs there is indeed a strong
 337 negative feedback between the solar and volcanic forcings. This is seen more clearly in Fig. 3c which shows that at $\Delta t \approx 400$
 338 years, that the negative feedback is strong enough to reduce the theoretical additive fluctuation amplitudes by a factor of ≈ 2 (the
 339 fall-off at the largest Δt is probably an artefact of the poor statistics at these scales). It should be noted that in addition to
 340 linearity, the latter holds assuming statistical independence (top curve in Fig. 3c) of the solar and volcanic forcing. For
 341 comparison, the bottom curve in Fig. 3c illustrates the results obtained when analyzing the series constructed by directly
 342 summing the two response series (instead of assuming statistical independence). It is clearly seen that the basic result still holds
 343 but it is a little less strong (a factor of ≈ 1.5). The reason for the difference is that the cancellation of the cross terms assumed by
 344 statistical independence is only approximately valid on single realizations, especially at the lower frequencies where the statistics
 345 are worse (even on a single realization, at any given scale - except the very longest - there are several fluctuations so that there is
 346 still some averaging).

347 The calculations above ignored the model's internal variability, this was considered small due to the averaging over 100
 348 realizations of the ZC model with the same forcings: the internal is expected to largely cancel out. While it is true that a
 349 definitive answer to this requires running the model in "control mode" so as to capture only the internal variability (as was done
 350 in for the GISS model, see Fig. 4), there are nevertheless several reasons why the internal variability is almost certainly smaller
 351 than the response due to the forcings:

- 352 i) We can get a typical order of magnitude of the internal variability from the GISS model, Fig. 4; we see that for a
 353 single realization - without averaging over 100 realizations as in Fig. 3a – that the typical centennial variability is \approx
 354 $\pm 0.05\text{K}$ and decreasing with a power law with exponent $\approx \xi(2) / 2 \approx -0.2$. After averaging for 100 realizations, we
 355 expect this to decrease by $(100)^{0.5} = 10$, i.e. to $\pm 0.005\text{K}$. This is much smaller than the centennial scale variability
 356 of the ZC responses in Fig. 3a (from the graph, these are about $\approx \pm (10^{-1.2}) / 2 \approx \pm 0.03\text{K}$).
- 357 ii) We can use the fact that a) the observed responses are upper bounds on the internal variability and b) that the
 358 internal variability must decrease with scale (otherwise the model's climate diverges rather than converges for long
 359 times. Exponents near the GISS value $\xi(2) / 2 \approx -0.2$ are common, see e.g. Lovejoy et al., (2013). From Fig. 2, we
 360 see that the ZC solar response at ≈ 20 years is $\pm 0.03\text{K}$, so this is an upper bound for the internal variability at all
 361 scales longer than ≈ 20 years. However, over the range $\approx 50\text{-}500$ years (relevant for the subadditivity conclusion),
 362 the solar response variability is considerably larger than this noise value: from the graph, $\approx \pm (10^{-0.8}) / 2 \approx \pm 0.08\text{K}$.

363 We conclude that it is unlikely that the internal variability is strong enough to account for the results.

364 In the ZC model, all forcings are input at the surface so that here the subadditivity is due to the differing
 365 seasonality, fluctuation intensities and spatial distributions of the solar and volcanic forcings. In the GISS-E2-R GCM
 366 simulations, the response to the solar forcing is too small to allow us to determine if it involves a similar solar-volcanic negative
 367 feedback (Fig. 4). In GCMs with their vertically stratified atmospheres or the real atmosphere, non additivity is perhaps not
 368 surprising given the difference between the solar and volcanic vertical heating profiles. If such negative feedbacks are
 369 substantiated in further simulations, it would enhance the credibility of the idea that current GCMs are missing critical slow
 370 (multi centennial, multi millennial) climate processes. No matter what the exact explanation, non additivity underlines the
 371 limitations of the convenient reduction of climate forcings to radiative forcing equivalents. It also indicates that at scales longer
 372 than about 50 yrs energy budget models must nonlinearly account for albedo-temperature interactions (i.e. that linear energy
 373 budget models are inadequate at these time scales, and that albedo-temperature interactions must at least be correctly
 374 parametrized).

375 Also shown for reference in Fig. 3a are the fluctuations for three multiproxy estimates of annual northern hemisphere
 376 temperatures (1500-1900; pre-industrial, Moberg et al., 2005; Huang, 2004; Ljungqvist, 2010, the analysis was taken from
 377 Lovejoy and Schertzer, 2012c). Although it should be borne in mind that the ZC model region (the Pacific) does not coincide
 378 with the proxy region (the northern hemisphere), the latter is the best model validation available. In addition, since we compare
 379 model and proxy fluctuation statistics as functions of time scale, the fact that the spatial regions are somewhat different is less
 380 important than if we had attempted a direct year by year comparison of model outputs with the multiproxy reconstructions.

381 In Fig. 3a, we see that the responses of the volcanic only and the combined volcanic and solar forcings fairly well
 382 reproduce the RMS multiproxy statistics until ≈ 50 yrs; however at longer time scales, the model fluctuations are substantially
 383 too weak – roughly 0.1 K (corresponding to ± 0.05 K) and constant or falling, whereas at 400 yr scales, the RMS multiproxy
 384 temperature fluctuations are ≈ 0.25 K (± 0.125) and rising. Indeed, in order to account for the ice ages, they must continue to rise
 385 until ≈ 5 K (± 2.5 K) at glacial-interglacial scales of 50 – 100 kyr, (the “glacial-interglacial window”: according to paleodata,
 386 this rise continues in a smooth, power law manner with $H>0$ until roughly 100 kyr, see Lovejoy and Schertzer, 1986, Shackleton
 387 and Imbrie, 1990 Pelletier, 1998, Schmitt et al., 1995, Ashkenazy et al., 2003, Huybers and Curry, 2006, and Lovejoy et al.,
 388 2013).

389 In Fig. 4, we compare the RMS Haar fluctuations from the ZC model combined (volcanic and solar forcing) response
 390 with those from simulations from the GISS-E2-R GCM with solar only forcing and a control run (no forcings, black; see
 391 Lovejoy et al., (2013) for details; the GISS-E2-R solar forcing was the same as the spliced series used in the ZC simulations).
 392 We see that the three are remarkably close over the entire range; for the GISS model, this indicates that the solar only forcing is
 393 so small that the response is nearly the same as for the unforced (control) run. The ZC combined solar and volcanic forcing is
 394 clearly much weaker than the pre-industrial multiproxies (dashed blue, same as in Fig. 3a). The reference line with slope -0.2
 395 shows the convergence of the control to the model climate; the shallowness of the slope (-0.2) implies that the convergence is
 396 ultra slow. For example, fluctuations from a 10 yr run control run are only reduced by a factor of $(10/3000)^{-0.2} \approx 3$ if the run is
 397 extended to 3 kyr.

398 Finally, in Fig. 5, we compare the responses to the volcanic forcings for the Zebiak-Cane model and for the GISS-E2-R
 399 GCM for two different volcanic reconstructions (Gao et al., 2008), and Crowley, 2000) (the reconstruction used in the ZC
 400 simulation). For reference, we again show the combined ZC response and the preindustrial multiproxies. We see that the GISS
 401 GCM is much more sensitive to the volcanic forcing than the Zebiak-Cane model; indeed, it is too sensitive at scales $\Delta t \approx 100$,

102 but nevertheless becomes too weak at scales $\Delta t \approx 200$ years. Indeed, since the volcanic forcings continue to
 103 decrease with scale, we expect the responses to keep diminishing with scale at larger Δt .

104 Note that the spatial regions covered by the ZC simulation, the GISS outputs and the multiproxy reconstructions are not
 105 the same. For the latter, the reason is that there is no perfectly appropriate (regionally defined) multiproxy series whereas for the
 106 GISS outputs, we reproduced the structure function analysis from a published source. Yet, the differences in the regions may not
 107 be so important since we are only making statistical comparisons. This is especially true since all the series are for planetary
 108 scale temperatures (even if they are not identical global sized regions) and in addition, we are mostly interested in the fifty year
 109 (and longer) statistics which may be quite similar.

110 **4. Intermittency: a multifractal trace moment analysis**

111 **4.1 The Trace moment analysis technique**

112 In the previous sections we considered the implications of linearity when climate models were forced separately with two
 113 different forcings compared with the response to the combined forcing; we showed that the ZC model was subadditive. However,
 114 linearity also constrains the relation between the fluctuations in the forcings and the responses. For example at least since the
 115 work of Clement et al., (1996), in the context of volcanic eruptions, it has been recognized that the models are typically sensitive
 116 to weak forcing events but insensitive to strong ones, i.e. they are nonlinear, and Mann et al., (2005) noticed this in their ZC
 117 simulations.

118 In a scaling regime, both forcings and responses will be characterized by a hierarchy of exponents (i.e. the function $\xi(q)$
 119 in Eq. 3 or equivalently by the exponent H and the function $K(q)$), the differences in the statistics of weak and strong events are
 120 reflected in these different exponents; high order moments (large q) are dominated by large fluctuations and conversely for low
 121 order moments. The degree of convexity of $K(q)$ quantifies the degree of these nonlinear effects (indeed, how they vary over
 122 time scales Δt). Such “intermittent” behaviour was first studied in the context of turbulence (Kolmogorov, 1962; Mandelbrot,
 123 1974).

124 In order to quantify this, recall that if the system is linear, the response is a convolution of the system Green’s function
 125 with the forcing, in spectral terms it acts as a filter. If it is also scaling, then the filter is a power law: ω^{-H} where ω is the
 126 frequency, (mathematically, if $\mathcal{F}(\omega)$ and $\mathcal{F}_F(\omega)$ are the Fourier transforms of the response and forcing, for a scaling linear
 127 system, we have: $\mathcal{F}(\omega) \propto \omega^{-H} \mathcal{F}_F(\omega)$ such a filter corresponds to a fractional integration of order H). In terms of fluctuations this
 128 implies: $\Delta T(\Delta t) = \Delta t^H \Delta F(\Delta t)$ (assuming that the fluctuations are appropriately defined). Therefore, by taking q^{th} powers of both
 129 sides and ensemble averaging, we see that in linear scaling systems we have: $\xi_T(q) = qH + \xi_F(q)$ (c.f. eq. (3) with $\xi_T(q)$ and
 130 $\xi_F(q)$ the structure function exponents for the response and the forcing respectively). If $\xi_T(q)$ and $\xi_F(q)$ only differ by a term
 131 linear in q , then $K_T(q) = K_F(q)$, so that if over some regime, we find empirically $K_T(q) \neq K_F(q)$ (i.e. the intermittencies are
 132 different), then we may conclude that that the system is nonlinear (note that this result is independent of whether the linearity is
 133 deterministic or only statistical in nature).

134 Let us investigate the nonlinearity of the exponents by returning to Eq. (1), (2) and (3) in more detail. Up until

135 now we have studied the statistical properties of the forcings and responses using the RMS fluctuations e.g. we have used the

136 following equation but only for the value $q = 2$:

$$137 \quad \langle \Delta T(\Delta t)^q \rangle \propto \langle \varphi_{\lambda'}^q \rangle \Delta t^{qH} = \Delta t^{\xi(q)}; \quad \xi(q) = qH - K(q) \quad (6)$$

138 (see Eq. (1)) the exponent $K(q)$ (implicitly defined in (3)) is given explicitly by:

$$139 \quad \langle \varphi_{\lambda'}^q \rangle = \Delta t^{K(q)}; \quad \frac{\tau_{eff}}{\Delta t} \quad (7)$$

140 where τ_{eff} is the effective outer scale of the multifractal cascade process, φ gives rise to the strong variability and λ' is the
141 cascade ratio from this outer scale to the scale of interest Δt .

142 If the driving flux φ was quasi-Gaussian, then $K(q)=0$, $\xi(q)=qH$ and the exponent $\xi(2)=2H=\beta-1$ would be
143 sufficient for a complete characterization of the statistics. However geophysical series are often far from Gaussian, even without
144 statistical analysis, a visual inspection (the sharp spike" of varying amplitudes, see Fig. 1a) of the volcanic series makes it
145 obvious that it is particularly extreme in this regard. We expect - at least in this case - that the $K(q)$ term will readily be quite
146 large (although note the constraint $K(1)=0$ and the mean of φ (the $q=1$ statistic) is independent of scale). To characterize this,
147 note that since $K(1)=0$, we have $\xi(1)=H$ and then use the first two derivatives of $\xi(q)$ at $q=1$ to estimate the tangent (linear
148 approximation) to $K(q)$ near the mean (C_1) and the curvature of $K(q)$ near the mean characterized by α . This gives

$$149 \quad \left. \begin{aligned} C_1 &= K'(1) = H - \xi'(1) \\ \alpha &= K''(1) / K'(1) = \xi''(1) / (\xi'(1) - H) \end{aligned} \right\} \quad (8)$$

150 The parameters C_1 , α are particularly convenient since – thanks to a kind of multiplicative central limit theorem - there

151 exist multifractal universality classes (Schertzer and Lovejoy, 1987). For such universal multifractal processes, the exponent

152 function $K(q)$ can be entirely (i.e. not only near $q=1$) characterized by the same two parameters:

$$153 \quad K(q) = \frac{C_1}{\alpha-1} (q^\alpha - q); \quad 0 \leq \alpha \leq 2 \quad (9)$$

154 In the universality case (9), it can be checked that the estimate in (8) (near the mean) is satisfied so that C_1 , α

155 characterize all the statistical moments (actually, (6), (7) are only valid for $q < q_c$; for $q > q_c$, the above will break down due to
156 multifractal phase transitions; the critical q_c is typically >2 , so that here we confine our analyses to $q \leq 2$ and do not discuss the
157 corresponding extreme - large q - behaviour).

158 A drawback of the above fluctuation method for using $\xi(q)$ to estimate $K(q)$ (6) is that if C_1 is not too big, then for the

159 low order moments q , the exponent $\xi(q)$ may be dominated by the linear (qH) term, so that the multifractal part ($K(q)$) of the
160 scaling is not too apparent. A simple way of directly studying $K(q)$ is to transform the original series so as to estimate the flux φ
161 at a small scale, essentially removing the (qH) part of the exponent. It can then be degraded by temporal averaging and the

162 scaling of the various statistical moments - the exponents $K(q)$ - can be estimated directly. To do this, we divide (1) by
 163 its ensemble average so as to estimate the normalized flux at the highest resolution by:

$$164 \quad \varphi' = \frac{\varphi}{\langle \varphi \rangle} = \frac{\Delta T}{\langle \Delta T \rangle} \quad (10)$$

165 where the ensemble average (“ $\langle \rangle$ ”) is estimated by averaging over the available data (here a single series), and the fluctuations
 166 Δt are estimated at the finest resolution (here 1 yr).

167

168

169 **4.2 Trace moment analysis of forcings, responses and multiproxies**

170 We now test (7); for convenience, we use the symbol λ as the ratio of a convenient reference scale – here the length of
 171 the series, $\tau_{ref} = 1000$ yrs to the resolution scale Δt (for some analyses, 400 yrs was used instead, see the captions in Fig. 6). In
 172 an empirical study, the outer scale τ_{eff} is not known a priori, it must be empirically estimated; denote the scale at which the
 173 cascade starts by λ'

174 Starting with (7), the basic prediction of multiplicative cascades is that the normalized moments φ' (10) obey the generic
 175 multiscaling relation:

$$176 \quad M(q) = \langle \varphi_{\lambda}^{q'} \rangle = \lambda'^{K(q)} = \left(\frac{\tau_{eff}}{\Delta t} \right)^{K(q)} = \left(\frac{\lambda}{\lambda_{eff}} \right)^{K(q)}; \lambda' = \frac{\tau_{eff}}{\Delta t} = \frac{\lambda}{\lambda_{eff}}; \lambda_{eff} = \frac{\tau_{ref}}{\tau_{eff}} \quad (11)$$

177 We can see that τ_{eff} can readily be empirically estimated since a plot of $\text{Log}_{10}M$ versus $\text{Log}_{10}\lambda$ will have lines (one for
 178 each q , slope $K(q)$) converging at the outer scale $\lambda = \lambda_{eff}$ (although for a single realisation such as here, the outer scale will
 179 be poorly estimated since clearly for a single sample (series) there is no variability at the longest time scales, there is a single
 180 long-term value that generally poorly represents the ensemble mean). Figure 6a shows the results when ΔT is estimated by the
 181 absolute second difference at the finest resolution. The solar forcing (upper right) was only shown for the recent period (1600-
 182 2000) over which the higher resolution sunspot based reconstruction was used, the earlier 1000-1600 part was based on a (too)
 183 low resolution ^{10}Be “splice” as discussed above, see Fig. 2b. In the solar plot (upper left), but especially in the volcanic forcing
 184 plot (upper right), we see that the scaling is excellent over nearly the entire range (the points are nearly linear) and in addition,
 185 the lines plausibly “point” (i.e. cross) at a unique outer scale $\lambda = \lambda_{eff}$ which is not far from the length of the series, see Table
 186 1 for estimates of the corresponding time scales. From these plots we see that the responses to the volcanic forcing “spikiness”
 187 (intermittency) are much stronger than to the corresponding responses to the weaker solar “spikiness”. The model atmosphere
 188 therefore considerably dampens the intermittency, but in addition this effect is highly nonlinear so that the intermittency of the
 189 combined volcanic and solar forcing (bottom left) is actually a little less than the volcanic only intermittency (bottom right).
 190 Table 1 gives a quantitative characterization of the intermittency strength near the mean, using the C_1 parameter.

191 It is interesting at this stage to compare the intermittency of the ZC outputs with those of the GISS-E2-R GCM (Fig. 6b)
 192 and with multiproxy temperature reconstructions (Fig. 6c). In Fig. 6b, we see that the GISS-E2-R trace moments rapidly die off
 193 at large scales (small λ) so that the intermittency is limited to small scales to the right of the convergence point. In this Figure,

194 we see that the lines converge at $\text{Log}_{10}\lambda \approx 1.1-1.5$ corresponding to τ_{eff} in the range roughly 10–30 yrs. Since the
 195 intermittency builds up scale by scale from large scales modulating smaller scales in a hierarchical manner, and since this range
 196 of scales is small, the intermittency will be small. The partial exception is for the upper right plot which is for the GISS-E2-R
 197 response to the large Gao volcanic forcing (recall that the ZC model uses the weaker, Crowley volcanic reconstruction whose
 198 response is strongly intermittent, see Fig. 6b, the upper left plot). This result shows that contrary to the ZC model whose
 199 response is strongly intermittent (highly non Gaussian) over most of the range of time scales, the GISS-E2-R response is nearly
 200 Gaussian implying that the (highly non Gaussian) forcings are quite heavily (nonlinearly) damped.

201 This difference in the model responses to the forcing intermittency is already interesting, but it does not settle the question
 202 as to which model is more realistic. To attempt to answer this question, we turn to Fig. 6c which shows the trace moment
 203 analysis for six multiproxy temperature reconstructions over the same (pre-industrial) period as the GISS-E2-R model (1500–
 204 1900; unlike the ZC model, the GISS-E2-R included anthropogenic forcings so that the period since 1900 was not used in the
 205 GISS-E2-R analysis). Statistical comparisons of nine multiproxies were made in ch. 11 of Lovejoy and Schertzer, (2013), (for
 206 reasons of space, only six of these are shown in Fig. 6c) where it was found that the pre 2003 multiproxies had significantly
 207 smaller multicentennial and lower frequency variability than the more recent multiproxies used as reference in Fig. 4 and 5.
 208 However, Fig. 6c shows that the intermittencies are all quite low (with the partial exception of the Mann series, see the upper
 209 right plot). This conclusion is supported by the comparison with the red curves. These indicate the generic envelope of trace
 210 moments of quasi-Gaussian processes for $q \leq 2$ it shows how the latter converge (at large scales, small λ , to the left) to the
 211 flat ($K(q) = 0$) Gaussian limit. We see that the actual lines are only slightly outside this envelope showing that they are only
 212 marginally more variable than quasi-Gaussian processes.

213 The comparison of the GISS-E2-R outputs (Fig. 6b) with the multiproxies (Fig. 6c) indicates that they are both of low
 214 intermittency and are more similar to each other than to the ZC multiproxy statistics. One is therefore tempted to conclude that
 215 the GISS-E2-R model is more realistic than the ZC model with its much stronger intermittency. However this conclusion may be
 216 premature since the low multiproxy and GISS intermittencies may be due to limitations of both the multiproxies and the GISS-
 217 E2-R model. Multicentennial and multimillennial scale ice core analyses displays significant paleotemperature intermittency (
 218 $C_1 \approx 0.05-0.1$, Schmitt et al., 1995 see the discussion in ch. 11 of Lovejoy and Schertzer, 2013) so that the multiproxies may be
 219 insufficiently intermittent.

520 5. Conclusions

521 From the point of view of GCM's, climate change is a consequence of changing boundary conditions (including composition),
 522 the latter are the climate forcings. Since forcings of interest (such as anthropogenic forcings) are typically of the order of 1% of
 523 the mean solar input the responses are plausibly linear. This justifies the reduction of the forcings to a convenient common
 524 denominator: the “equivalent radiative forcing”, a concept which is useful only if different forcings add linearly, if they are
 525 “additive”. An additional consequence of linearity is that the climate sensitivities are independent of whether the fluctuations in
 526 the forcings are weak or strong. Both consequences of linearity clearly have their limits. For example, at millennial and longer
 527 scales, energy balance models commonly discard linearity altogether and assume that nonlinear albedo responses to orbital

528 changes are dominant. Similarly, at monthly and annual scales, the linearity of the climate sensitivity has been
 529 questioned in the context of sharp, strong volcanic forcings.

530 In view of the widespread use of the linearity assumption, it is important to quantitatively establish its limits and this can
 531 best be done using numerical climate models. A particularly convenient context is provided by the Last Millennium simulations,
 532 which (in the preindustrial epoch) are primarily driven by the physically distinct solar and volcanic forcings (forcings due to land
 533 use changes are very weak). The ideal would be to have a suite of the responses of fully coupled GCM's which include solar
 534 only, volcanic only and combined solar and volcanic forcings and control runs (for the internal variability) so that the responses
 535 could be evaluated both individually and when combined. Unfortunately, the optimal set of GCM products are the GISS E2-R
 536 millennium simulations with solar only and solar plus volcanic forcing and a control run (this suite is missing the volcanic only
 537 responses). We therefore also considered the outputs of a simplified climate model, the Zebiac-Cane (ZC) model (Mann et al.,
 538 2005) for which the full suite of external forcing response was available.

539 Following a previous study, we first quantified the variability of the forcings as a function of time scale by considering
 540 fluctuations. These were estimated by using the difference between the averages of the first and second halves of intervals Δt
 541 ("Haar" fluctuations). This definition was necessary in order to capture the two qualitatively different regimes, namely those in
 542 which the average fluctuations increase with time scale ($H > 0$) and those in which they decrease with scale ($H < 0$). Whereas the
 543 solar forcing was small at annual scales, it generally increased with scale. In comparison, the volcanic forcing was very strong at
 544 annual scales but rapidly decreased, the two becoming roughly equal at about 200 yrs. By considering the response to the
 545 combined forcing we were then able to examine and quantify their non-additivity (nonlinearity). By direct analysis (Fig. 3b, c), it
 546 was found that in the ZC model, additivity of the radiative forcings only works up until roughly 50 yr scales; at 400 yr scales,
 547 there are negative feedback interactions between the solar and volcanic forcings that reduce the combined effect by a factor of \approx
 548 1.5 - 2. This "subadditivity" makes their combined effects particularly weak at these scales. Although this result seems
 549 statistically robust for the ZC Millennium simulations, until the source of the nonlinearity is pin-pointed and the results
 550 reproduced with full-blown coupled GCM's, they must be considered tentative (the conclusions would also be strengthened if
 551 ZC control runs output were available to estimate the internal variability), many more simulations with diverse forcings are
 552 needed to completely settle the issue..

553 In order to investigate possible nonlinear responses to sharp, strong events (such as volcanic eruptions), we used the fact
 554 that if the system is linear and scaling, then the difference between the structure function exponents ($\xi(q)$) for the forcings and
 555 responses is itself a linear function of the order of moment q (moments with large q are mostly sensitive to the rare large
 556 values, small q moments are dominated by the frequent low values). By using the trace moment analysis technique, we isolated
 557 the nonlinear part of $\xi(q)$ (i.e. the function $K(q)$) which quantifies the intermittent (multifractal, highly non-Gaussian) part of the
 558 variability (associated with the "spikiness" of the signal). Unsurprisingly we showed that the volcanic intermittency was much
 559 stronger than the solar intermittency, but that in both cases, the model responses were highly smoothed, they were practically
 560 nonintermittent (close to Gaussian) hence that the model responses to sharp, strong events were not characterized by the same
 561 sensitivity as to the more common weaker forcing events.

562 By examining model outputs, we have found evidence that the response of the climate system is reasonably linear with
 563 respect to the forcing up to time scales of 50 yrs at least for weak (i.e. not sharp, intermittent) events. But the sharp, intermittent
 564 events such as volcanic eruptions that occasionally disrupt the linearity at shorter time scales, become rapidly weaker at longer

565 and longer time scales (with scaling exponent $H \approx -0.3$). In practice, linear stochastic models may therefore be valid
 566 from over most of the macroweather range, from ≈ 10 days to over 50 years. However, given their potential importance, it would
 567 be worth designing specific coupled climate model experiments in order to investigate this further.
 568

569 **6. Acknowledgements:**

570 The ZC simulation outputs and corresponding solar and volcanic forcings were taken from
 571 ftp://ftp.ncdc.noaa.gov/pub/data/paleo/climate_forcing/mann2005/mann2005.txt. We thank J. Lean (solar data Fig. 2b (top),
 572 Judith.Lean@nrl.navy.mil), A. Shapiro (solar data, Fig. 2b (bottom) Alexander Shapiro, alexander.shapiro@pmodwrc.ch) and G.
 573 Schmidt (the GISS-E2-R simulation outputs, gavin.a.schmidt@nasa.gov) for graciously providing data and model outputs. The
 574 ECHAM5 based Millennium simulations analyzed in table 1 were available from: https://www.dkrz.de/Klimaforschung-en/konsortial-en/millennium-experiments-1?set_language=en. Mathematica and MatLab codes for performing the Haar
 576 fluctuation analyses are available from: <http://www.physics.mcgill.ca/~gang/software/index.html>. This work was unfunded, there
 577 were no conflicts of interest.

578 **References**

579 Anderson, J. L.: A method for producing and evaluating probabilistic forecasts from ensemble model integrations, *J. Climate*, 9,
 580 1518–1530, 1996.

581 Ashkenazy, Y., D. Baker, H. Gildor, and Havlin, S.: Nonlinearity and multifractality of climate change in the past 420,000 years,
 582 *Geophys. Res. Lett.*, 30, 2146 doi: 10.1029/2003GL018099, 2003

583 Blender, R., and Fraedrich, K.: Comment on “Volcanic forcing improves atmosphere–ocean coupled general circulation model
 584 scaling performance” by D. Vyushin, I. Zhidkov, S. Havlin, A. Bunde, and S. Brenner, *Geophys. Res. Lett.*, 31, L22213,
 585 doi: 10.1029/2004GL020797, 2004.

586 Bothe, O., Jungclaus, J. H., and Zanchettin, D.: Consistency of the multi-model CMIP5/PMIP3-past1000 ensemble, *Climate of
 587 the Past*, 9 (6), 2471-2487, 2013a.

588 Bothe, O., Jungclaus, J. H., Zanchettin, D., and Zorita, E.: Climate of the last millennium: Ensemble consistency of simulations
 589 and reconstructions, *Climate of the Past*, 9 (3), 1089-1110, 2013b.

590 Bryson, R. A.: The Paradigm of Climatology: An Essay, *Bull. Amer. Meteor. Soc.*, 78, 450-456, 1997.

591 Budyko, M. I.: The effect of solar radiation variations on the climate of the earth, *Tellus*, 21, 611-619, 1969.

592 Bunde, A., Eichner, J. F., Kantelhardt, J. W, and Havlin, S.: Long-term memory: a natural mechanism for the clustering of
 593 extreme events and anomalous residual times in climate records, *Phys. Rev. Lett.*, 94, 1-4 doi:
 594 10.1103/PhysRevLett.94.048701, 2005.

595 Chandra, S., Varotsos, C., and Flynn, L. E. The mid-latitude total ozone trends in the northern hemisphere, *Geophys Res Lett.*,
 596 23(5), 555-558, 1996.

597 Clement, A. C., Seager, R., Cane, M. A., and Zebiak, S. E.: An ocean dynamical thermostat, 2190–2196, 1996.

598 Cracknell, A. P., and Varotsos, C. A.: New aspects of global climate-dynamics research and remote sensing. *Int. J. Remote Sens.*,
 599 32(3), 579-600, 2011.

600 Cracknell, A. P., & Varotsos, C. A.: The Antarctic 2006 ozone hole. *Int. J. Remote Sens.*, 28(1), 1-2, 2007.

501 Crowley, T. J. :Causes of Climate Change Over the Past 1000 Years, Science, 289, 270 doi:
 502 10.1126/science.289.5477.270, 2000.

503 Dijkstra, H.: *Nonlinear Climate Dynamics*, 357 pp., Cambridge University Press, Cambridge, 2013.

504 Efstatthiou, M. N., Tzanis, C., Cracknell, A. P., and Varotsos, C. A.: New features of land and sea surface temperature anomalies.
 505 Int. J. Remote Sens., 32(11), 3231-3238, 2011.

506 Eichner, J. F., Koscielny-Bunde, E., Bunde, A., Havlin, S., and Schellnhuber, H.-J.: Power-law persistance and trends in the
 507 atmosphere: A detailed studey of long temperature records, Phys. Rev. E, 68, 046133-046131-046135 doi:
 508 10.1103/PhysRevE.68.046133, 2003.

509 Fraedrich, K., Blender, R., and Zhu, X.: Continuum Climate Variability: Long-Term Memory, Scaling, and 1/f-Noise,
 510 International Journal of Modern Physics B, 23, 5403-5416, 2009.,

511 Franzke, J., Frank, D., Raible, C. C., Esper, J., and Brönnimann, S.: Spectral biases in tree-ring climate proxies Nature Clim.
 512 Change, 3, 360-364 doi: doi: 10.1038/Nclimate1816, 2013.

513 Fredriksen, H.-B., and Rypdal, K.: Scaling of Atmosphere and Ocean Temperature Correlations in Observations and Climate
 514 Models, J. Climate doi: doi.org/10.1175/JCLI-D-15-0457.1, 2015.

515 Gao, C. G., Robock, A., and Ammann, C.: Volcanic forcing of climate over the past 1500 years: and improved ice core-based
 516 index for climate models, J. Geophys. Res., 113, D23111 doi: 10.1029/2008JD010239, 2008.

517 Goswami, B. N., and Shukla, J.: Aperiodic Variability in the Cane—Zebiak Model, J. of Climate, 6, 628-638, 1991.

518 Hansen, J., Sato, M. K. I., Ruedy, R., Nazarenko, L., Lacis, A., Schmidt, G. A., and Bell, N.: Efficacy of climate forcings, J.
 519 Geophys. Res., 110, D18104 doi:10.1029/2005JD005776, 2005.

520 Hasselmann, K.: Stochastic Climate models, part I: Theory, Tellus, 28, 473-485, 1976

521 Huang, S.: Merging Information from Different Resources for New Insights into Climate Change in the Past and Future,
 522 Geophys. Res., 31, L13205 doi:10.1029/2004 GL019781, 2004.

523 Hurst, H. E.: Long-term storage capacity of reservoirs, Trans. Amer. Soc. Civil Eng., 116, 770-808, 1951.

524 Huybers, P., and Curry, W.: Links between annual, Milankovitch and continuum temperature variability, Nature, 441, 329-332
 525 doi:10.1038/nature04745, 2006.

526 Kantelhardt, J. W., Koscielny-Bunde, E., Rybski, D., Braun, P., Bunde, A., and Havlin, S.: Long-term persistence and
 527 multifractality of precipitation and river runoff record, J. Geophys. Res., 111 doi: doi:10.1029/2005JD005881, 2006.

528 Kolesnikov, V. N., and Monin, A. S.: Spectra of meteorological field fluctuations, Izvestiya, Atmospheric and Oceanic Physics,
 529 1, 653-669, 1965.,

530 Kolmogorov, A. N.: A refinement of previous hypotheses concerning the local structure of turbulence in viscous incompressible
 531 fluid at high Raynolds number, Journal of Fluid Mechanics, 83, 349, 1962,

532 Kondratyev, K. Y., and Varotsos, C. A.: Volcanic eruptions and global ozone dynamics, Int. J. Remote Sens., 16 (10), 1887-
 533 1895, 1995a.

534 Kondratyev, K. Y., and Varotsos, C. A.: Atmospheric greenhouse - effect in the context of global climate-change NUOVO
 535 CIMENTO DELLA SOCIETA ITALIANA DI FISICA C-GEOPHYSICS AND SPACE PHYSICS 18, 123-151, 1995b

536 Koscielny-Bunde, E., Bunde, A., Havlin, S., Roman, H. E., Goldreich, Y., and Schellnhuber, H. J.: Indication of a universal
 537 persistence law governing atmospheric variability, Phys. Rev. Lett. , 81, 729-732, 1998.

538 Krivova, N. A., Balmaceda, L., and Solanski, S. K.: Reconstruction of solar total irradiance since 1700 from the
 539 surface magnetic field flux, *Astron. and Astrophys.*, 467, 335-346 doi: 10.1051/0004-6361:20066725, 2007.

540 Laepple, T., Jewson, S., and Coughlin, K.: Interannual temperature predictions using the CMIP3 multi-model ensemble mean,
 541 *Geophys. Res. Lett.*, 35, L10701, doi:10.1029/2008GL033576, 2008.

542 Lean, J. L.: Evolution of the Sun's Spectral Irradiance Since the Maunder Minimum, *Geophys. Res Lett.*, 27, 2425-2428, 2000.

543 Lean, J. L., and Rind, D. H.: How natural and anthropogenic influences alter global and regional surface temperatures: 1889 to
 544 2006, *Geophys. Res. Lett.*, 35, L18701 doi: 10.1029/2008GL034864, 2008.

545 Ljungqvist, F. C.: A new reconstruction of temperature variability in the extra - tropical Northern Hemisphere during the last two
 546 millennia, *Geografiska Annaler: Physical Geography*, 92 A(3), 339 - 351 doi:10.1111/j.1468 - 0459.2010 .00399.x, 2010.

547 Lovejoy, S.: What is climate?, *EOS*, 94, (1), 1 January, p1-2, 2013.

548 Lovejoy, S.: Scaling fluctuation analysis and statistical hypothesis testing of anthropogenic warming, *Climate Dyn.*, 42, 2339-
 549 2351 doi:10.1007/s00382-014-2128-2, 2014a.

550 Lovejoy, S.: A voyage through scales, a missing quadrillion and why the climate is not what ou expect, *Climate Dyn.*, 44, 3187-
 551 3210, doi: 10.1007/s00382-014-2324-0, 2014b.,

552 Lovejoy, S.: The macroweather to climate transition in the Holocene: regional and epoch to epoch variability (comments on
 553 "Are there multiple scaling regimes in Holocene temperature records?" by T. Nilsen, K. Rypdal, and H.-B. Fredriksen),
 554 *Earth Syst. Dynam. Discus.*, 6, C1-C10, 2015a.

555 Lovejoy, S.: Using scaling for macroweather forecasting including the pause, *Geophys. Res. Lett.*, 42, 7148-7155
 556 doi:10.1002/2015GL065665, 2015b.

557 Lovejoy, S., and Schertzer, D.: Scale invariance in climatological temperatures and the local spectral plateau, *Annales
 558 Geophysicae*, 4B, 401-410, 1986.,

559 Lovejoy, S., and Schertzer,D.: Towards a new synthesis for atmospheric dynamics: space-time cascades, *Atmos. Res.*, 96, 1-52
 560 doi:10.1016/j.atmosres.2010.01.004, 2010.

561 Lovejoy, S., and Schertzer, D.: Stochastic and scaling climate sensitivities: solar, volcanic and orbital forcings, *Geophys. Res.
 562 Lett.*, 39, L11702, doi:10.1029/2012GL051871, 2012a.,

563 Lovejoy, S., and Schertzer, D.: Low frequency weather and the emergence of the Climate, in *Extreme Events and Natural
 564 Hazards: The Complexity Perspective*, edited by A. S. Sharma, A. Bunde, D. N. Baker and V. P. Dimri, pp. 231-254,
 565 AGU monographs, Washington D.C., 2012b,

566 Lovejoy, S., and Schertzer, D.: Haar wavelets, fluctuations and structure functions: convenient choices for geophysics,
 567 *Nonlinear Proc. Geophys.*, 19, 1-14, doi:10.5194/npg-19-1-2012, 2012c.

568 Lovejoy, S., and Schertzer, D.: The Weather and Climate: Emergent Laws and Multifractal Cascades, 496 pp., Cambridge
 569 University Press, Cambridge, 2013.

570 Lovejoy, S., Schertzer, D., and Varon, D.: Do GCM's predict the climate.... or macroweather?, *Earth Syst. Dynam.* , 4, 1-16
 571 doi:10.5194/esd-4-1-2013, 2013.,

572 Lovejoy, S., Muller, J. P., and Boisvert, J. P.: On Mars too, expect macroweather, *Geophys. Res. Lett.*, 41, 7694-7700,
 573 doi:10.1002/2014GL061861, 2014.

574 Lovejoy, S., del Rio Amador, L., and Hébert, R.: The ScaLIng Macroweather Model (SLIMM): using scaling to
 575 forecast global-scale macroweather from months to Decades, *Earth Syst. Dynam.*, 6, 1–22, <http://www.earth-syst-dynam.net/6/1/2015/>, doi:10.5194/esd-6-1-2015, 2015.

577 Mandelbrot, B. B.: Intermittent turbulence in self-similar cascades: divergence of high moments and dimension of the carrier,
 578 *Journal of Fluid Mechanics*, 62, 331-350, 1974.

579 Mann, M. E., Cane, M. A., Zebiak, S. E., and Clement, A.: Volcanic and solar forcing of the tropical pacific over the past 1000
 580 years, *J. Clim.*, 18, 447-456, 2005.

581 Marzban, C., Wang, R., Kong, F., and Leyton, S.: On the effect of correlations on rank histograms: reliability of temperature and
 582 wind speed forecasts from fine scale ensemble reforecasts, *Mon. Weather Rev.*, 139, 295–310,
 583 doi:doi:10.1175/2010MWR3129.1, 2011.

584 Meehl, G. A., Washington, W. M., Ammann, C. M., Arblaster, J. M., Wigley, T. M. L., and Tebaldi, C.: Combinations Of
 585 Natural and Anthropogenic Forcings In Twentieth-Century Climate, *J. of Clim.* , 17, 3721-3727, 2004.

586 Miller, G. H., Geirsdóttir, Á., Zhong, Y., Larsen, D. J., Otto Bliesner, B. L., Holland, M. M., and Anderson, C.: Abrupt onset of
 587 the Little Ice Age triggered by volcanism and sustained by sea-ice/ocean feedbacks, *Geophys. Res. Lett.*, 39, L02708
 588 doi:10.1029/2011GL050168, 2012.

589 Minnis, P., Harrison, E. F., Stowe, L. L., Gibson, G. G., Denn, F. M., Doelling, D. R., and Smith Jr, W. L.: Radiative Climate
 590 Forcing by the Mount Pinatubo Eruption, *Science*, 259 (5100), 1411-1415, 1993.

591 Moberg, A., Sonnechkin, D. M., Holmgren, K., Datsenko, N. M., and Karlén, W.: Highly variable Northern Hemisphere
 592 temperatures reconstructed from low- and high - resolution proxy data, *Nature*, 433(7026), 613-617, 2005.

593 Newman, M.: An Empirical Benchmark for Decadal Forecasts of Global Surface Temperature Anomalies, *J. of Clim.*, 26, 5260-
 594 5269, doi:10.1175/JCLI-D-12-00590.1, 2013.

595 Newman, M. P., Sardeshmukh, P. D., and Whitaker, J. S.: A study of subseasonal predictability, *Mon. Wea. Rev.*, 131, 1715-
 596 1732, 2003.

597 Nicolis, C.: Transient climatic response to increasing CO₂ concentration: some dynamical scenarios, *Tellus A*, 40A, 50-60,
 598 doi:10.1111/j.1600-0870.1988.tb00330.x, 1988.

599 Østvand, L., Nilsen, T., Rypdal, K., Divine, D., and Rypdal, M.: Long-range memory in millennium-long ESM and AOGCM
 700 experiments, *Earth System Dynamics*, 5, ISSN 2190-4979.s 2295 - 2308.s, doi:10.5194/esd-5-295-2014, 2014.

701 Panofsky, H. A., and Van der Hoven, I.: Spectra and cross-spectra of velocity components in the mesometeorological range,
 702 Quarterly J. of the Royal Meteorol. Soc., 81, 603-606, 1955.

703 Pelletier, J., D.: The power spectral density of atmospheric temperature from scales of 10⁻² to 10⁶ yr, *EPSL*, 158, 157-164, 1998.

704 Peng, C.-K., Buldyrev, S. V., Havlin, S., Simons, M., Stanley, H. E., and Goldberger, A. L.: Mosaic organisation of DNA
 705 nucleotides, *Phys. Rev. E*, 49, 1685-1689, 1994..

706 Penland, C., and Sardeshmukh, P. D.: The optimal growth of tropical sea surface temperature anomalies, *J. Climate*, 8, 1999-
 707 2024, 1995.

708 Pielke, R.: Climate prediction as an initial value problem, *Bull. of the Amer. Meteor. Soc.*, 79, 2743-2746, 1998.

709 Ragone, F., Lucarini, V., and Lunkeit, F.: A new framework for climate sensitivity and prediction: a modelling perspective,
 710 *Climate Dynamics*, 1-13, 2014.

711 Roques, L., Chekroun, M. D., Cristofol, M., Soubeyrand, S., and Ghi, M.: Parameter estimation for energy balance
712 models with memory, *Proc. Roy. Soc. A*, 470 20140349 doi: DOI: 10.1098/rspa.2014.0349, 2014.

713 Rybski, D., Bunde, A. Havlin, S., and von Storch, H.: Long-term persistance in climate and the detection problem, *Geophys.*
714 *Resear. Lett.*, 33, L06718-06711-06714, doi:10.1029/2005GL025591, 2006.

715 Rypdal, M., and Rypdal, K.: Long-memory effects in linear response models of Earth's temperature and implications for future
716 global warming, *J. Climate*, 27 (14), 5240 - 5258, doi:10.1175/JCLI-D-13-00296.1, 2014.

717 Sardeshmukh, P. D., and Sura, P.: Reconciling non-gaussian climate statistics with linear dynamics, *J. of Climate*, 22, 1193-
718 1207, 2009.

719 Schertzer, D., and Lovejoy, S.: Physical modeling and Analysis of Rain and Clouds by Anisotropic Scaling of Multiplicative
720 Processes, *J Geophys Res*, 92, 9693-9714, 1987.

721 Schmidt, G. A., et al.: Using paleo-climate model/data comparisons to constrain future projections in CMIP5, *Clim. Past*
722 *Discuss.*, 9, 775-835, doi:10.5194/cpd-9-775-2013, 2013.

723 Schmitt, F., Lovejoy, S., and Schertzer, D.: Multifractal analysis of the Greenland Ice-core project climate data., *Geophys. Res.*
724 *Lett*, 22, 1689-1692, 1995.

725 Shackleton, N. J., and Imbrie, J.: The $\delta^{18}\text{O}$ spectrum of oceanic deep water over a five-decade band, *Climatic Change*, 16, 217-
726 230, 1990.

727 Shapiro, A. I., Schmutz, W., Rozanov, E., Schoell, M., Haberreiter, M., Shapiro, A. V., and Nyeki, S.: A new approach to long-
728 term reconstruction of the solar irradiance leads to large historical solar forcing, *Astronomy & Astrophysics*, 529, A67,
729 doi: doi.org/10.1051/0004-6361/201016173, 2011.

730 Shindell, D. T., Schmidt, G. A., Miller, R. I., and Mann, M. E.:Volcanic and Solar Forcing of Climate Change during the
731 Preindustrial Era, *J. Clim.*, 16, 4094-4107, 2003.

732 Steinhilber, F., Beer, J., and Frohlich, C.: Total solar irradiance during the Holocene, *Geophys. Res. Lett.*, 36, L19704,
733 doi:10.1029/2009GL040142, 2009.

734 Van der Hoven, I.: Power spectrum of horizontal wind speed in the frequency range from 0.0007 to 900 cycles per hour, *Journal*
735 *of Meteorology*, 14, 160-164, 1957.

736 Varotsos, C. A.: The global signature of the ENSO and SST-like fields. *Theor. Applied Clim.*, 113(1-2), 197-204, 2013.

737 Varotsos, C., Efstatthiou, M., and Tzanis, C.: Scaling behaviour of the global tropopause. *Atmos Chem Phys*, 9(2), 677-683, 2009.

738 Varotsos, C., Kalabokas, P., and Chronopoulos, G.: Association of the laminated vertical ozone structure with the lower-
739 stratospheric circulation. *J. Applied Meteorol*, 33(4), 473-476, 1994.

740 Vyushin, D., Zhidkov, I., Havlin, S., Bunde, A., and Brenner, S.: Volcanic forcing improves atmosphere-ocean coupled, general
741 circulation model scaling performance. *Geophy. Res. Lett.*, 31, L10206, doi:10.1029/2004GL019499, 2004.

742 Wang, Y.-M., Lean, J. L., and Sheeley, N. R. J.: Modeling the Sun's magnetic field and irradiance since 1713, *Astrophys J.* ,
743 625, 522-538, 2005.

744 Watson, A. J. and Lovelock, J. E.: Biological homeostasis of the global environment: the parable of Daisyworld, *Tellus*, 35B,
745 284-289, 1983.

746 Weber, S. L.: A timescale analysis of the Northern Hemisphere temperature response to volcanic and solar forcing, *Climate of*
747 *the Past*, 1, 9-17, 2005.

748 Zanchettin, D., Rubino, A., and Jungclaus, J. H.: Intermittent multidecadal-to-centennial fluctuations dominate global
 749 temperature evolution over the last millennium, *Geophys. Res. Lett.*, 37 (14), L14702, 2010.

750 Zanchettin, D., Rubino, A., Matei, D., Bothe, O., and Jungclaus, J. H.: Multidecadal-to-centennial SST variability in the MPI-
 751 ESM simulation ensemble for the last millennium, *Climate Dynamics*, 40 (5-6), 1301-1318, 2013.

752 Zebiak, S. E., and Cane, M. A.: A Model El Niño – Southern Oscillation, *Mon. Wea. Rev.*, 115, 2262–2278, 1987..

753 Zhu, X., Fraederich, L., and Blender, R.:Variability regimes of simulated Atlantic MOC, *Geophys. Res. Lett.*, 33, L21603,
 754 doi:10.1029/2006GL027291, 2006.

755

756 **Tables:**

757 **Table 1.** The scaling exponent estimates for the forcings and ZC model responses.

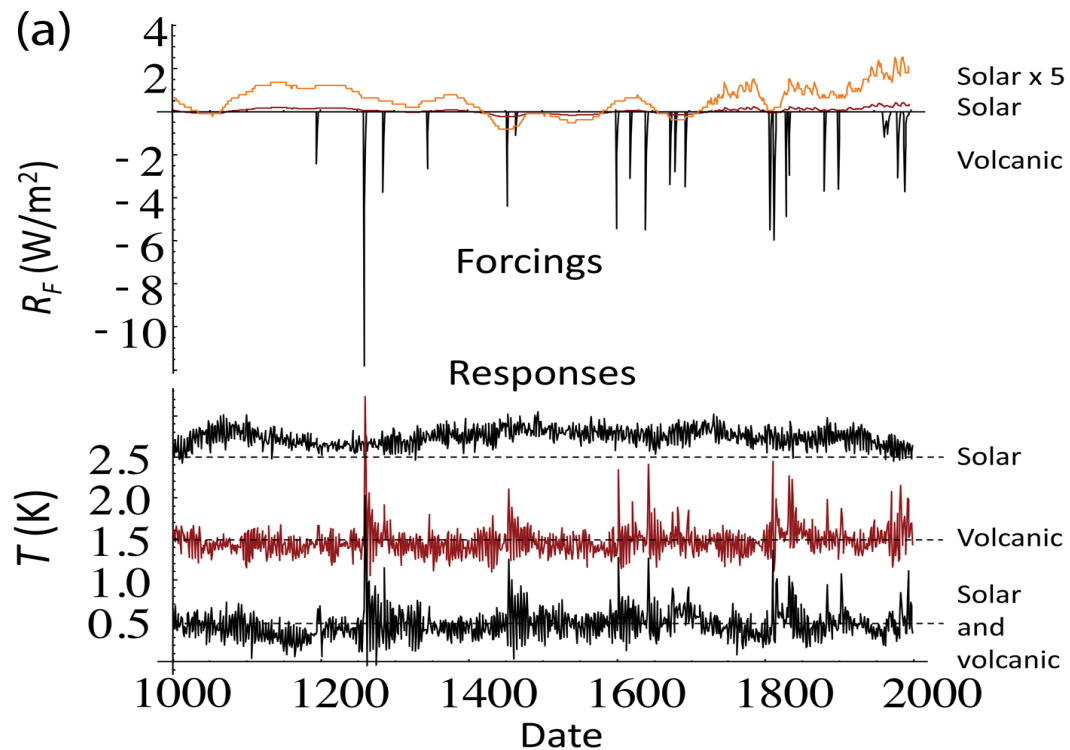
	Forcings		Responses			Control Runs	
	Solar	Volcanic	Solar	Volcanic	Combined	GISS	ECHAM5
H	0.40	-0.21	0.031	-0.17	-0.15	-0.26	-0.4
C_1	0.095	0.48	0.022	0.054	0.038	<0.01	<0.01
α	1.04	0.31	1.82	2.0	2.0	–	–
$\xi(2)/2$	0.33	-0.47	-0.01	-0.28	-0.23	<0.01	<0.01
β	1.66	0.06	0.98	0.44	0.54	0.47	0.2
τ_{eff}	630 yrs	300yrs	100yrs	100 yrs	250 yrs	–	–

758

759 Table 1 shows the scaling exponent estimates for the forcings and ZC model responses. For the solar (forcing and response), only
 760 the recent 400 yrs (sunspot based) series were used, for the others, the entire 1000 yrs range was used, see figure 6a. The RMS
 761 exponent was estimated from Eq. (6), (9): H was estimated from the Haar fluctuations, α , C_1 were estimated from the trace
 762 moments (Fig. 6a). Note that the external cascade scales are unreliable since they were estimated from a single realization. The
 763 control runs at the right are for the GISS-E2-R model discussed in the text and (ECHAM5) from the fully coupled COSMOS-
 764 ASOB Millenium long term simulations based on the Hamburg ECHAM5 model for 800–4000AD.

765

766

Figures and Captions:

767

768 **Figure 1a.** *Top graph:* The radiative forcings R_F (top, W/m^2) and responses $T(\text{K})$ from 1000-2000 AD for the Zebiak-Cane
 769 model, from Mann et al., (2005), integrated over the entire simulation region. The forcings are reconstructed solar (brown), solar
 770 blown up by a factor 5 (orange) and volcanic (red). For the solar forcing (top series), note the higher resolution and wandering
 771 character for the recent centuries – this part is based on sunspots, not ^{10}Be .

772 *Bottom graph:* The responses are for the solar forcing only (top), volcanic forcing only (middle) and both (bottom); they have
 773 been offset in the vertical for clarity by 2.5, 1.5, 0.5K, respectively.

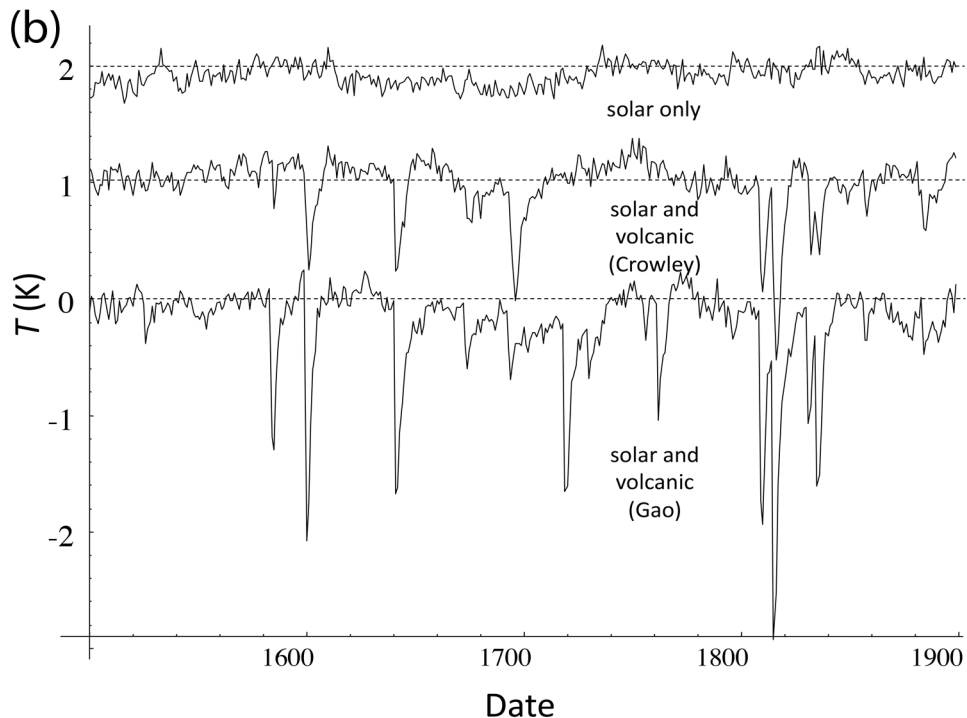
774

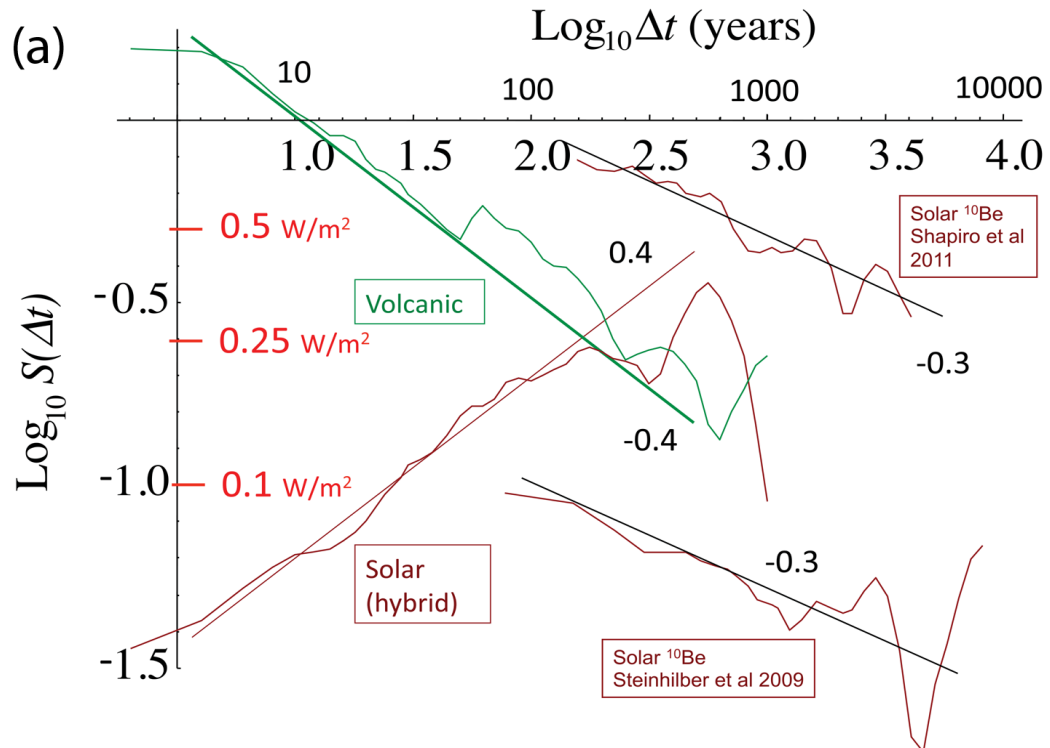
775

776

777

778



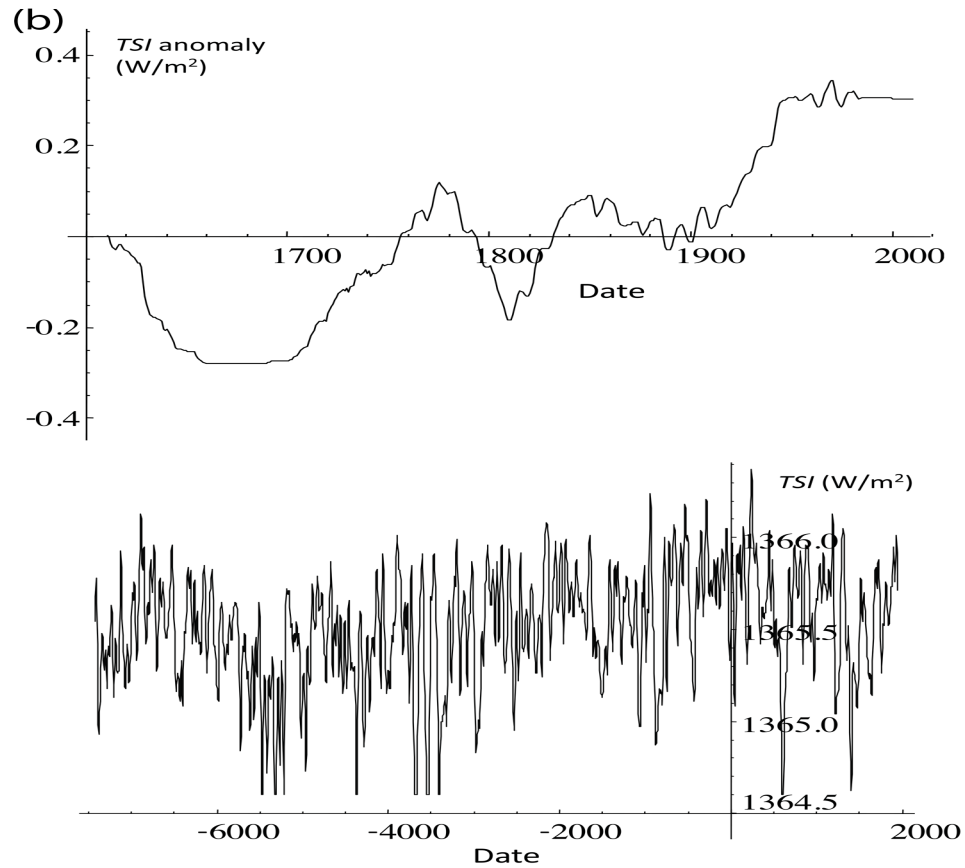


788

789 **Figure 2a.** The RMS Haar fluctuation $S(\Delta t)$ for the solar and volcanic reconstructions used in the ZC simulation for lags Δt from
 790 2 to 1000 years (left). The solar is a “hybrid” obtained by “splicing” the sunspot-based reconstruction (Fig. 2b, top) with a ^{10}Be
 791 based reconstruction (Fig. 2b, bottom). The two rightmost curves are for two different ^{10}Be reconstructions (Shapiro et al., 2011;
 792 Steinhilber et al., 2009). Although at any given scale, their different assumptions lead to amplitudes differing by nearly a factor
 793 of 10, their exponents are virtually identical and the amplitudes diminish rapidly with scale.

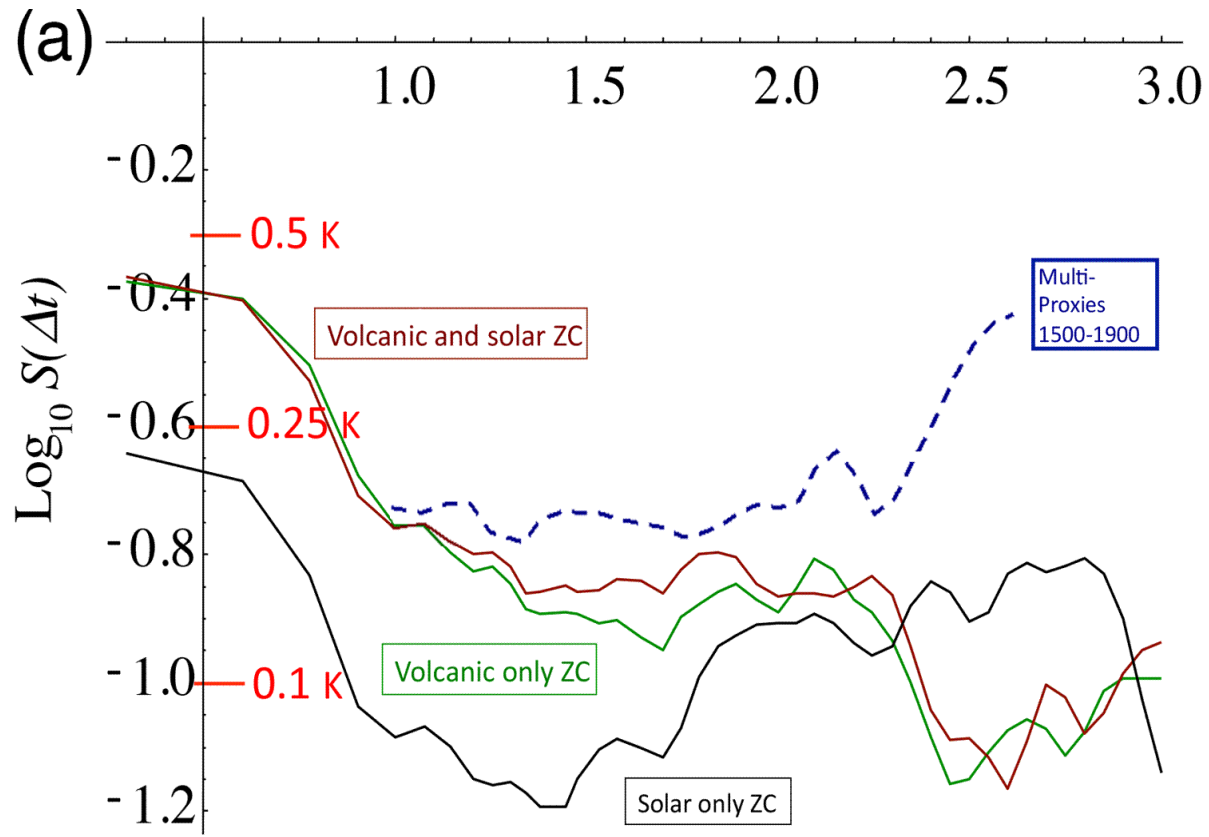
794

795



796

797 **Figure 2b.** A comparison of the sunspot derived Total Solar Irradiance (TSI) anomaly (top, used in the ZC and GISS simulations
 798 back to 1610, $H \approx 0.4$) with a recent ^{10}Be reconstruction (bottom, total TSI - mean plus anomaly - since 7362 BC, see Fig. 2a for
 799 a fluctuation analysis, $H \approx -0.3$) similar to that “spliced” onto the sunspot reconstruction for the period 1000-1610. We can see
 800 that the statistical characteristics are totally different with the sunspot variations “wandering” ($H > 0$) whereas the ^{10}Be
 801 reconstruction is “cancelling” ($H < 0$). The sunspot data were for the “background” (i.e. with no 11 year cycle, see Wang et al.,
 802 2005 for details), the data for the ^{10}Be curve were from Shapiro et al., (2011).
 803



304

305

306

307

Figure 3a. The RMS Haar fluctuations of the Zebiak–Cane (ZC) model responses (from an ensemble of 100 realizations) with volcanic only (green, from the updated Crowley reconstruction), solar only (black, using the sunspot based background (Wang et al., 2005), and both (brown). No anthropogenic effects were modelled. Also shown for reference are the fluctuations for three multiproxy series (blue, dashed, from 1500-1900, pre-industrial, the fluctuations statistics from the three series were averaged, this curve was taken from Lovejoy and Schertzer, 2012b). We see that all the combined volcanic and solar response of the model reproduces the statistics until scales of \approx 50-100 years; however at longer time scales, the model fluctuations are substantially too weak – roughly 0.1K (corresponding to ± 0.05 K) and constant or falling, whereas at 400 yr scales, the temperature fluctuations are ≈ 0.25 K (± 0.125) and rising.

315

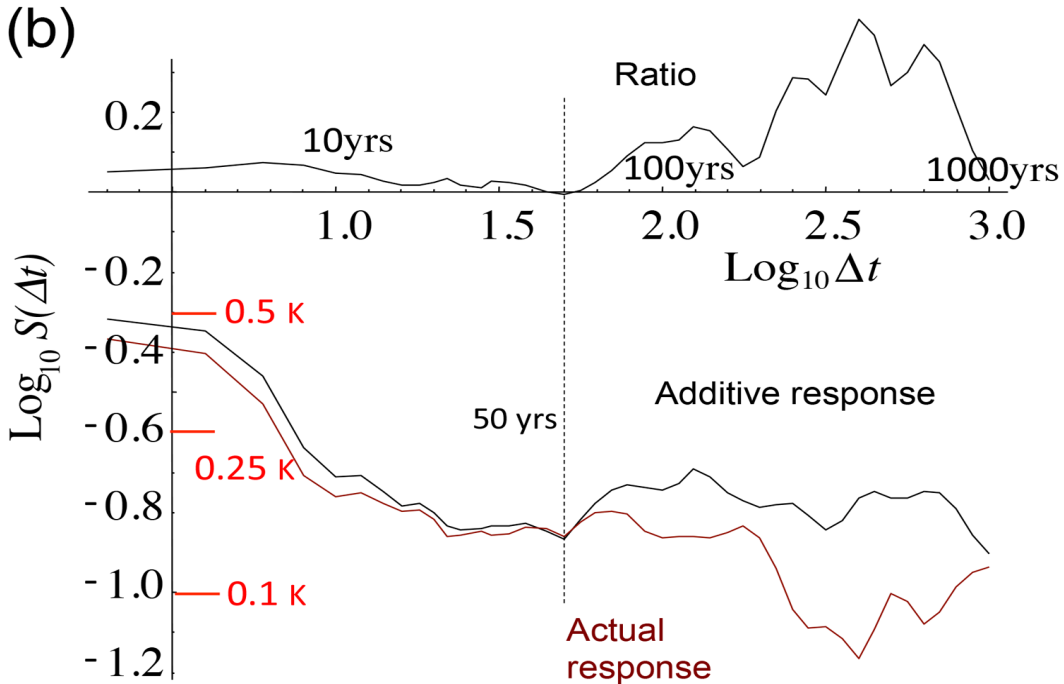
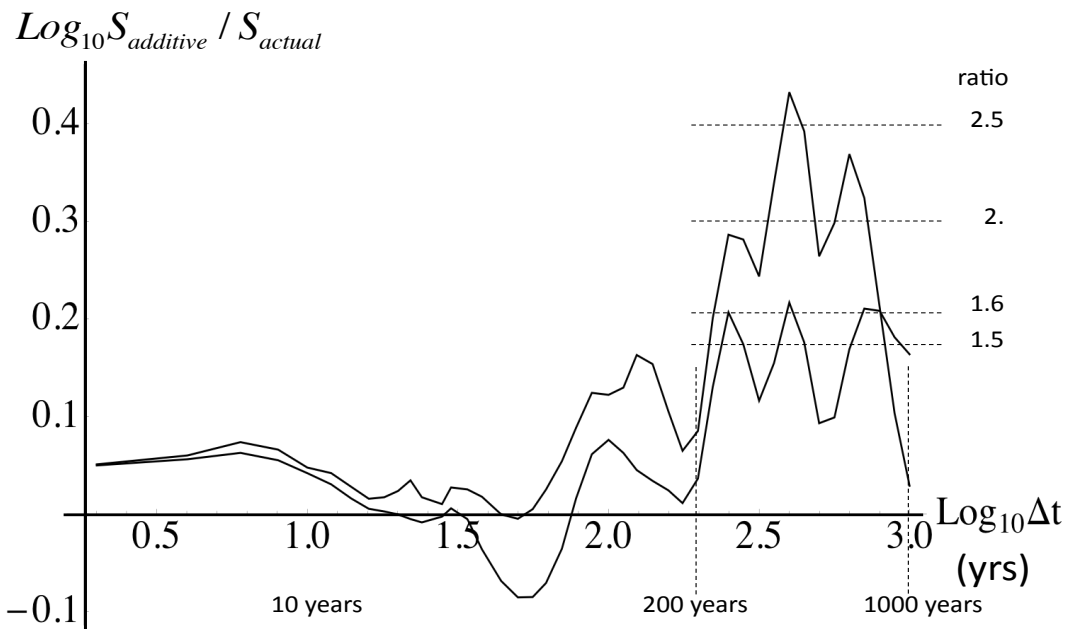


Figure 3b. A comparison of the RMS fluctuations of the ZC model response to combined solar and volcanic forcings (brown, bottom, from Fig. 3a), with the theoretical additive responses (black, bottom) as well as their ratio ($S_{\text{additive}} / S_{\text{actual}}$ black, top). The additive response was determined from the root mean square of the solar only and volcanic only response variances (from Fig. 3a): additivity implies that the fluctuation variances add (assuming that the solar and volcanic forcings are statistically independent). We can see that after about 50 years, there are strong negative feedbacks, the solar and volcanic forcings are subadditive, see Fig. 3c for a blow up of the ratio.

328

(C)

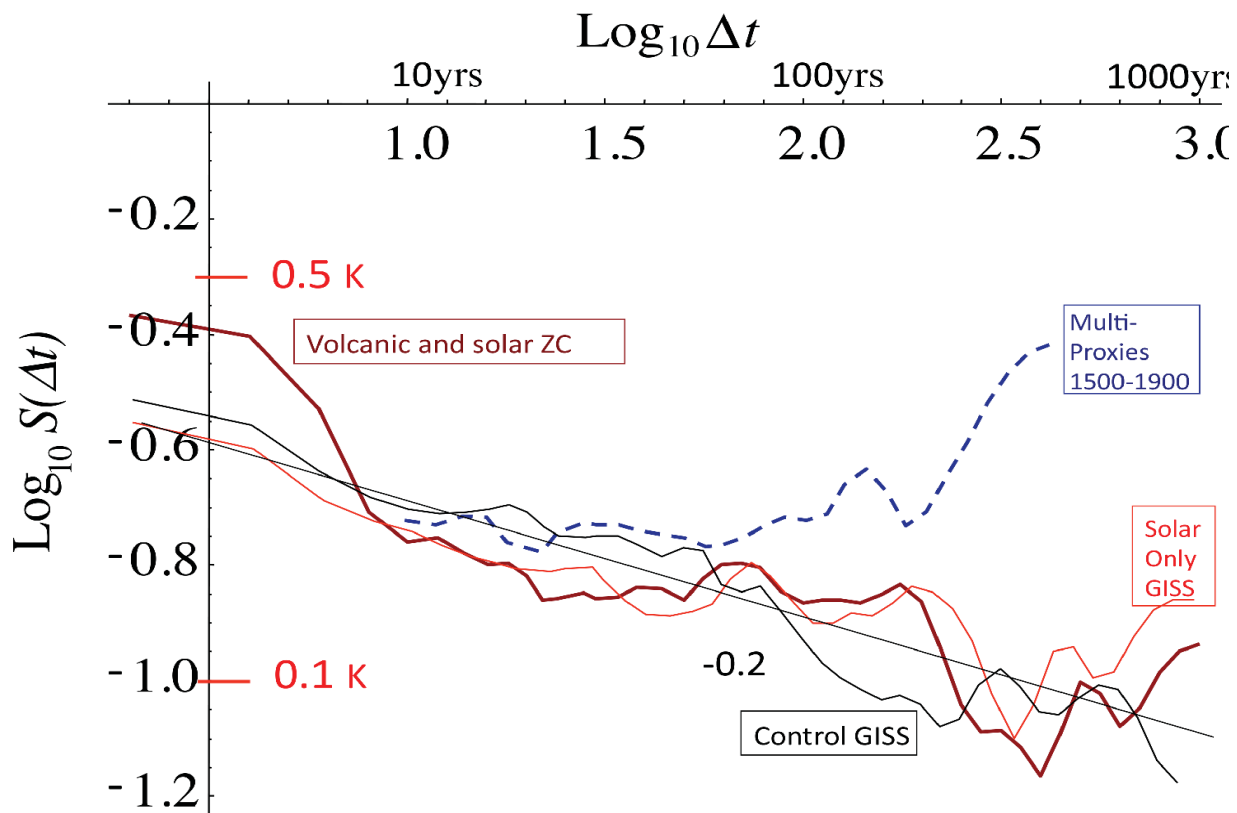


329

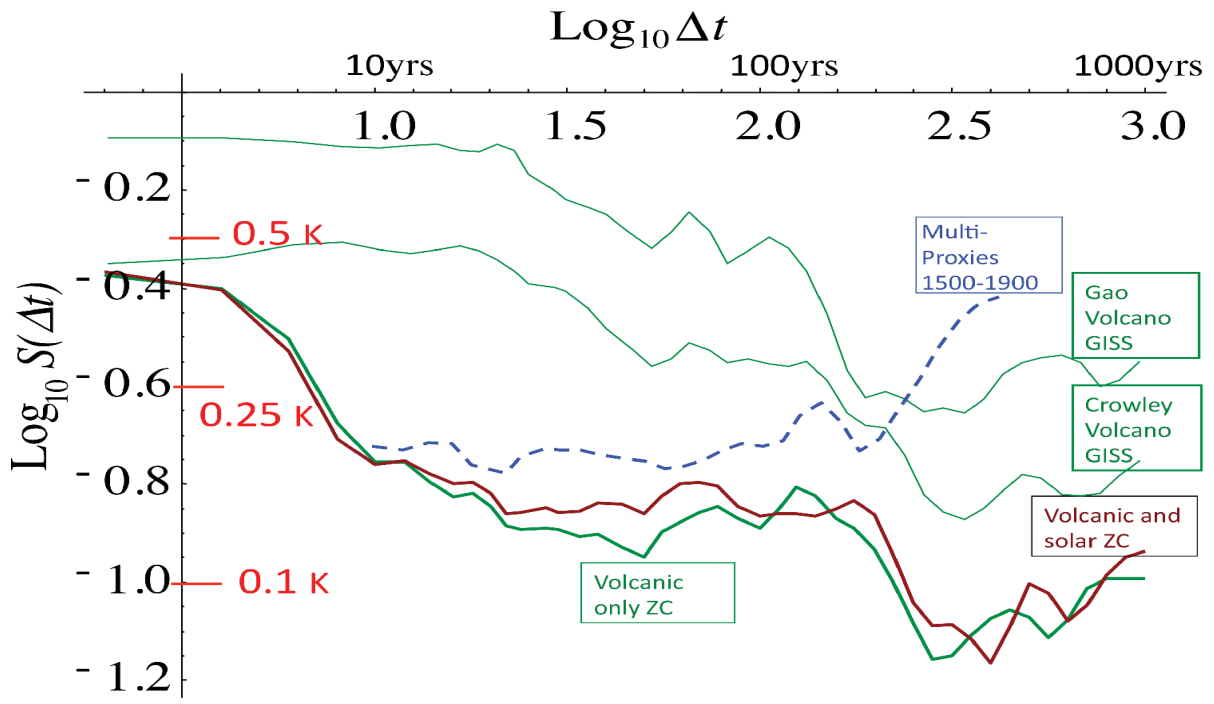
330 **Figure 3c.** An enlarged view of the ratio of the linear to nonlinear responses (from Fig. 3b). The top curve assumes for the
 331 combined forcing, the linearity of the response and statistical independence of the solar and volcanic forcings, whereas the
 332 bottom curve assumes only that the combined response to the forcing is linear uses the actual response to the combined forcings.
 333 The maximum at around 400 yrs (top curve) corresponds to a factor ≈ 2 (≈ 1.5 , bottom curve) of negative feedback between the
 334 solar and volcanic forcings. The decline at longer durations (Δt 's the single 1000 yr fluctuation) is likely to be an artefact of the
 335 limited statistics at these scales.

336

337



344

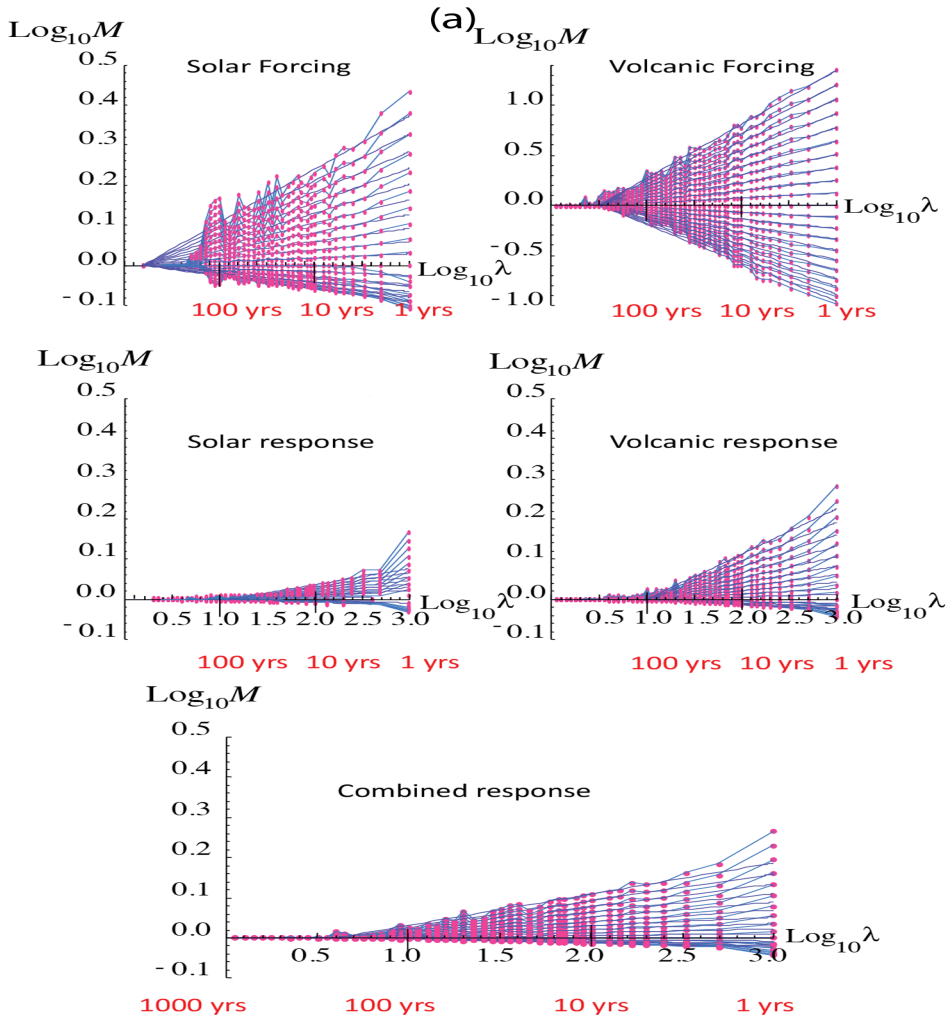


345

346

347 **Figure 5.** A comparison of the volcanic forcings for the ZC model (bottom green) and for the GISS-E2-R GCM for two different
 348 volcanic reconstructions (Gao et al., 2008, and Crowley, 2000) (top green curves, reproduced from Lovejoy et al., 2013). Also
 349 shown is the combined response (ZC, brown) and the preindustrial multiproxies (dashed blue).

350

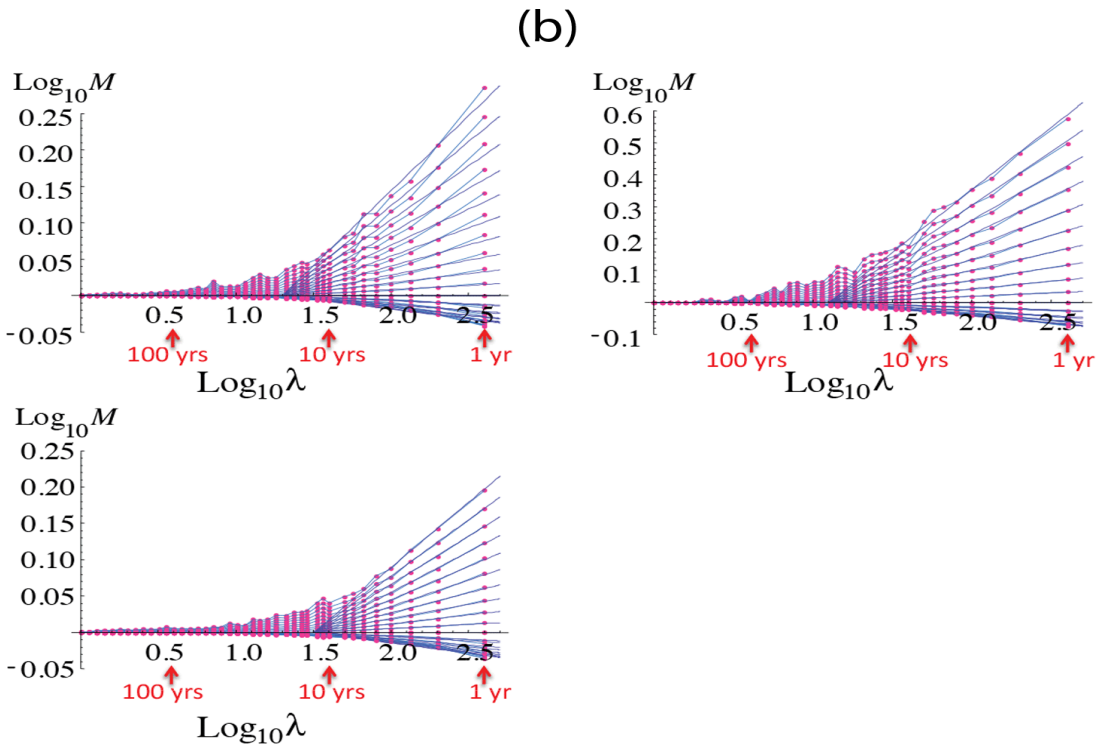


351

352

353 **Figure 6a.** Analysis of the fluxes/cascade structures of the ZC forcings (top row) and ZC temperature responses (middle, bottom
 354 rows); the normalized trace moments (Eq. (11)) are plotted for $q = 2, 1.9, 1.8, 1.7, 1.6, \dots, 0.1$. Upper left is solar forcing (last 400
 355 yrs only, mostly sunspot based), upper right is volcanic, middle left, solar response (last 400 yrs), middle right (volcanic
 356 response), lower left, response to combined forcings (last 1000 yrs). Note that all axes are the same except for volcanic. For the
 357 solar, only the last 400 yrs were used since this was reconstructed using the more reliable sunspot based method. The earlier ^{10}Be
 358 based reconstruction had relatively poor resolution and is not shown. Since the volcanic variability was so dominant, for the
 359 combined response (bottom left) the entire series was used. The red points and lines are the empirical values, the blue lines are
 360 regressions constrained to go through a single outer scale point, see eq. (11). In comparing the different parts of the figure, note
 361 in particular i) the log-log linearity for different statistical moments, ii) the fact that the lines for different moments reasonably
 362 cross at a single outer scale, and iii) the overall amplitude of the fluctuations – for example by visually comparing the range of
 363 the $q = 2$ moments (the top series) as we move from one graph to another.

364



365

366

367 **Figure 6b.** The above shows the responses for the GISS-E2-R simulations (northern hemisphere, land, 1500-1900), $\lambda=1$
 368 corresponds to 400 yrs. The upper left is for the response to the Crowley reconstructed volcanic forcings (same as used in the ZC
 369 simulations, not the change in the vertical scale), the upper right for the Gao reconstructed volcanic forcings and the lower left is
 370 for the solar only (mostly sunspot based, same as used in the ZC simulations).

371

372

373

374

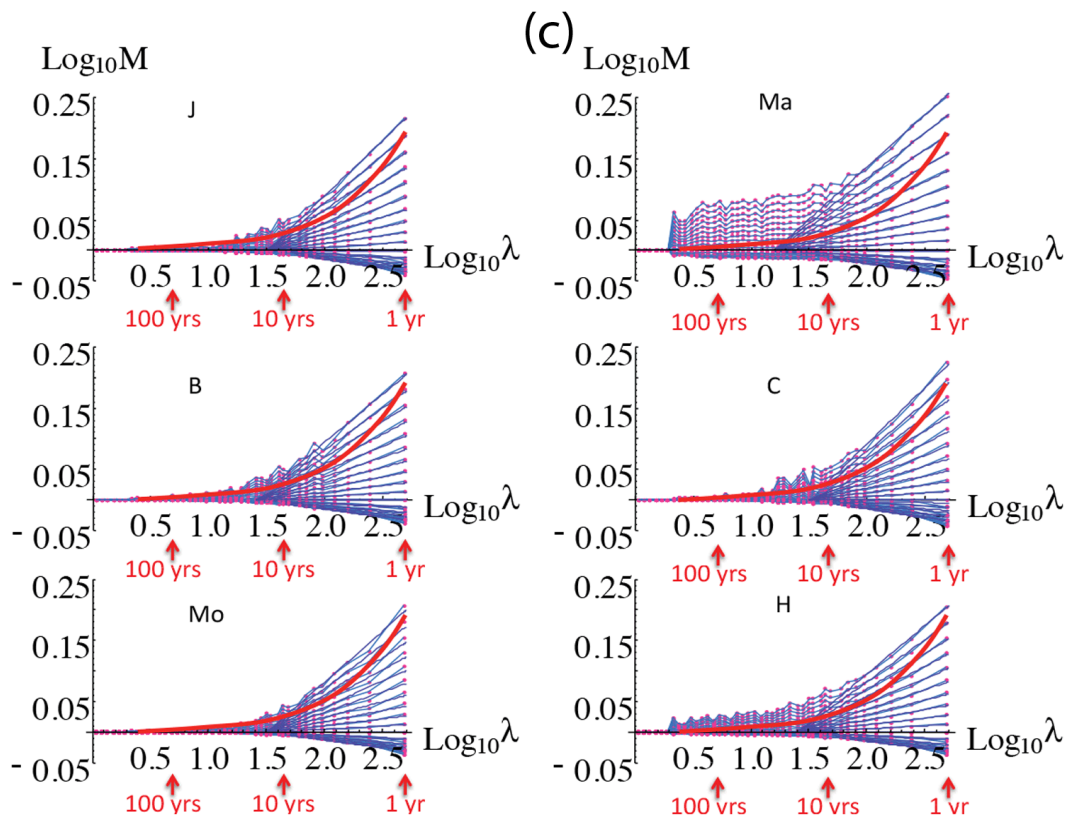
375

376

377

378

379



380

381

382 **Figure 6c.** Trace moment analysis of six annual resolution multiproxies, J = Jones, Ma = Mann 98, B = Briffa, C = Crowley, Mo
 383 = Moberg, H = Huang, the curves are reproduced with permission from figure 11.8, of Lovejoy and Schertzer, (2013), where full
 384 details and references are given. All were for the pre-industrial period 1500-1900 AD; $\lambda=1$ corresponds to 400 yrs. The curve
 385 shows the generic convergence of the envelope of curves to a quasi-Gaussian process, the proximity of the curve to the envelope
 386 indicates that with the possible exception of the Mann curve, the intermittency is low.